applied sciences

MDPI

Article

Effect of Ultrasonic Nanocrystal Surface Modification on the Structure, Mechanical Properties, and Tribological Behavior of Detonation-Sprayed NiCrAl Coatings

Maulet Meruyert [1], Zhuldyz Sagdoldina [1,*] and Nur Nabihah Yusof [2]

[1] Research Center "Surface Engineering and Tribology", Sarsen Amanzholov East Kazakhstan University, Ust-Kamenogorsk 070002, Kazakhstan; mauletmeruert@gmail.com
[2] School of Physics, Universiti Sains Malaysia, 11800 USM, Penang, Malaysia; nurnabihah7@usm.my
* Correspondence: zh.sagdoldina@gmail.com; Tel.: +7-747-663-6113

Abstract

The effect of ultrasonic nanocrystal surface modification (UNSM) on the structural-phase state, mechanical properties, and tribological behavior of detonation-sprayed NiCrAl coating was investigated. The UNSM treatment conditions are denoted as AxFy, where x represents the ultrasonic vibration amplitude A in μm and y represents the normal load F in N; for example, A30F10 corresponds to an amplitude of 30 μm and a normal load of 10 N. UNSM significantly reduced the surface roughness from Ra = 3.78 μm in the as-sprayed state to 0.25 μm for A40F10. X-ray diffraction showed that the principal AlNi, Al_4Ni_3, and $AlCr_2$ phases were retained after treatment, while weak Al_3Ni_5 reflections appeared under the A40F10 condition. SEM/EDS analysis confirmed preservation of the coating–substrate interface and revealed increased activation of inter-splat and subsurface defects at higher treatment intensity. The mean hardness remained comparable to the as-sprayed value under the moderate A20F10 and A30F10 conditions but decreased markedly under the more severe A40F10 and A10F20 conditions. Despite an increase in the coefficient of friction, wear resistance improved considerably. The minimum wear-track cross-sectional area of 1425 μm^2 was obtained for A30F10, representing an approximately 81% reduction compared with the as-sprayed coating. A30F10 provided the most favorable overall combination of surface smoothing, hardness, and wear resistance.

Keywords: NiCrAl coatings; detonation spraying; ultrasonic nanocrystal surface modification; UNSM; surface hardening; wear resistance; microstructure; tribology

Check for updates

Academic Editors: Noé López Perrusquia, Marco Antonio Doñu-Ruíz, Ernesto David Garcia Bustos and Milton Carlos Elías-Espinosa

Received: 18 August 2026
Revised: 8 September 2026
Accepted: 12 September 2026
Published: 16 September 2026

Copyright: © 2026 by the authors. Licensee MDPI, Basel, Switzerland. This article is an open access article distributed under the terms and conditions of the Creative Commons Attribution (CC BY) license.

1. Introduction

Surface hardening and the application of protective coatings are among the most effective methods for extending the service life of components operating under conditions of wear, oxidation, thermal cycling, and exposure to aggressive environments. In this context, Ni–Cr–Al system alloys combine several functionally significant components. The nickel matrix provides relatively high ductility, thermal stability, and compatibility with nickel- and iron-based structural materials; chromium promotes the formation of protective chromium-containing oxides and enhances resistance to hot corrosion; aluminum enables the formation of a slowly growing Al_2O_3-based oxide film. Therefore, Ni–Cr-based and related protective coating systems are widely used to improve oxidation, hot-corrosion, and wear resistance of components operating under severe thermal and mechanical conditions [1–4].

Detonation spraying is based on the cyclic combustion or detonation of a fuel–oxygen mixture in a barrel, during which powder particles are accelerated by a high-temperature gas flow and impact the prepared substrate at high velocity. Upon impact, the particles deform, form splats, and sequentially build up a layered coating. The high kinetic energy of the particles is one of the main features distinguishing the process from lower-velocity thermal spraying methods and promotes the formation of dense coatings with high adhesion strength. Compared with conventional plasma spraying, the detonation process can provide more intensive particle compaction upon impact, a lower fraction of large interlamellar voids, and high cohesive strength [5–7]. A significant advantage of the detonation method is the ability to control coating properties through the parameters of a single cycle: the fuel/oxygen ratio, barrel filling degree, powder feed amount, spraying distance, shot frequency, and number of passes.

Du et al. established a pronounced dependence of WC–Co coating quality on process variables, while Sundararajan et al. showed that the tribological behavior of detonation-sprayed coatings is determined not only by chemical composition but also by splat formation parameters, phase transformations, and defectiveness [8,9]. For gradient NiCr–Al_2O_3 coatings, a low barrel filling degree was accompanied by a less dense structure and a more heterogeneous surface topography, whereas an increase in spraying energy contributed to a reduction in the coefficient of friction and wear rate [10,11]. Recent investigations confirm the continuing interest in detonation-sprayed NiCrAl-based systems. Zhu et al. demonstrated that detonation-sprayed NiCrAlY/Al_2O_3/h-BN composite coatings can combine a dense structure and high bonding strength with favorable tribological performance over a wide temperature range [12]. Sagdoldina et al. further demonstrated that the mechanical and tribological properties of detonation-sprayed NiCr–Al coatings are strongly governed by their compositional architecture and resulting microstructure [13]. Despite the relatively high density and adhesion strength achievable by detonation spraying, the resulting coatings retain characteristic structural heterogeneities inherited from the particle-by-particle deposition mechanism. High-velocity particles undergo different degrees of heating, melting, flattening, and solidification upon impact, leading to the formation of splats separated by inter-splat boundaries. Locally incomplete spreading or bonding of adjacent particles can generate interlamellar discontinuities, pores, microvoids, and weakly bonded regions, while surface preparation and non-uniform particle impact may also produce isolated defects at the coating–substrate interface [5–11]. These features are intrinsic to thermally sprayed coatings and may remain even when the overall porosity is low. In addition, differences in local phase composition, particle thermal history, and rapid solidification can produce mechanically heterogeneous regions within the NiCrAl layer. Under subsequent contact loading, pores, splat boundaries, and interfacial discontinuities act as preferential sites for stress concentration and crack initiation. Therefore, the response of a detonation-sprayed coating to post-deposition mechanical treatment cannot be considered equivalent to that of a bulk metallic material.

This distinction is particularly important for ultrasonic nanocrystal surface modification. During UNSM, repeated high-frequency impacts generate cyclic normal and tangential contact stresses in the near-surface region. At moderate treatment intensity, these stresses can promote plastic flattening of surface asperities, local compaction of the coating, deformation hardening, and refinement of the near-surface structure. However, when the ultrasonic amplitude or static normal load exceeds the load-bearing capability of the lamellar coating architecture, the same repeated impacts may activate pre-existing pores and weak inter-splat boundaries, leading to crack opening, inter-splat separation, local chipping, and ultimately coating delamination. In such a case, an increase in treatment intensity does not necessarily result in further strengthening; instead, the accumulated structural

damage may reduce the effective resistance of the coating to indentation and subsequently decrease the measured hardness. Consequently, detonation-sprayed NiCrAl coatings are expected to exhibit a comparatively narrow UNSM processing window, determined by the balance between beneficial surface plastic deformation and damage accumulation within the heterogeneous coating structure. Consequently, a post-treatment method capable of smoothing the as-sprayed surface and strengthening the near-surface region without activating inherited defects or overloading the coating–substrate interface is required. Ultrasonic nanocrystal surface modification (UNSM) potentially meets these requirements, provided that the amplitude and normal load are carefully controlled.

During UNSM, a hard tip, typically made of tungsten carbide or another wear-resistant material, is pressed against the surface under a static load while simultaneously undergoing high-frequency oscillations. The sequence of impacts is generated by the controlled movement of the tip along parallel tracks. The UNSM processing conditions, including vibration amplitude, static load, treatment speed, tool geometry, and processing strategy, vary considerably among different materials and applications [14–18]. A gradient nanostructure and a favorable residual stress distribution were observed in 304 austenitic stainless steel after UNSM, providing a combination of high strength while maintaining ductility [19]. For AISI 304, it was established that the change in the residual stress state after UNSM improves fatigue strength [20]. A similar effect was observed for S45C steel, where the treatment was accompanied by surface hardening, the formation of compressive stresses, and an increase in fatigue life, as well as for SUS304 [21,22]. Comparison of UNSM with other intensive mechanical treatments of a nickel-based superalloy showed that different surface plastic deformation methods produce different deformation, microstructural, and residual stress profiles; therefore, the effect cannot be characterized solely by surface hardness [23]. UNSM has also been applied to Pt-modified aluminide coatings on Ni-based superalloys, where the mechanically modified surface state was shown to influence cyclic oxidation behavior [24].

More recent studies have extended the application of ultrasonic impact-based surface modification to coating systems. Amanov and Berkebile demonstrated that UNSM treatment of HVOF-sprayed Cr_2O_3 and Cr_3C_2–NiCr coatings reduced surface roughness, promoted grain refinement and surface hardening, and improved their tribological performance [25]. A subsequent study confirmed enhanced sliding wear and scratch resistance of thermally sprayed Cr-based coatings after UNSM [26]. More recently, UNSM treatment of HVOF-sprayed Al_2O_3–TiO_2 coatings was shown to smooth the coating surface, reduce the coefficient of friction, and enhance wear resistance under fuel-lubricated sliding conditions [27]. These findings demonstrate that the effectiveness of UNSM in sprayed coatings depends on the coupled evolution of surface topography, microstructure, mechanical response, and coating integrity.

The applicability of UNSM to sprayed coatings is therefore controlled not only by the intrinsic hardness of the deposited material, but also by the integrity of the splat network and the coating–substrate interface. The depth and intensity of the mechanically affected zone must remain compatible with the coating thickness and cohesive strength. If the imposed cyclic contact stresses are below the damage threshold, UNSM can promote surface smoothing, densification, deformation hardening, and compressive stress development. Conversely, excessive static load or ultrasonic amplitude can transfer a larger fraction of the impact energy into weak inter-splat and interfacial regions, promoting their opening and coalescence into larger crack-like discontinuities. Therefore, the optimal UNSM processing window for a sprayed coating is governed by the combined effects of coating thickness, porosity, inter-splat cohesion, interfacial adhesion, phase heterogeneity, and substrate support. Amanov A. investigated the application of UNSM to thermally sprayed ceramic

coatings on graphite and showed that the treatment can modify wear resistance and resistance to adhesive failure [28]. For a thermally sprayed Ni–Cr coating on carburized steel, UNSM improved the tribological behavior and adhesion strength of the system [29]. The latter study is a particularly close analogue for NiCrAl, as it confirms the compatibility of ultrasonic impact deformation with a metallic Ni–Cr-containing sprayed layer, although the spraying method, the presence of Al, and the initial microstructure differ. For Cr_2O_3 and Cr_3C_2–NiCr, improved tribological behavior after UNSM was demonstrated, while a subsequent study confirmed enhanced resistance to sliding wear and scratching of Cr-containing coatings [25,26]. For detonation-sprayed NiCrAl, crack formation, changes in open porosity, critical load during scratch testing, the failure characteristics of the wear track, and the condition of the coating–substrate interface should additionally be analyzed.

Recent studies further demonstrate that the improvement of surface and tribological properties cannot be attributed to a single parameter such as hardness or surface roughness, but instead results from the combined evolution of microstructure, phase constitution, interfacial integrity, and wear mechanisms. Li et al. reported a pronounced improvement in the wear resistance of laser-cladded AlCoCrFeNi high-entropy alloy coatings and related this behavior to the combined contribution of the coating microstructure, hard and soft constituent phases, and the formation of oxide-containing tribolayers during sliding [30]. Zhang et al. demonstrated that the mechanical and functional response of graphene-nanoplatelet-reinforced aluminum matrix composites produced by friction stir processing strongly depends on the processing-induced microstructural state [31]. A related study by Li et al. showed that the strengthening and toughening behavior of aluminum matrix composites is also strongly governed by microstructural evolution induced by hot rolling and friction stir processing [32]. These findings emphasize the importance of establishing processing–structure–property relationships when severe plastic deformation or surface modification is applied to structurally heterogeneous materials. However, these studies primarily concern bulk composites or coatings produced by laser-based processes, whereas the response of a lamellar detonation-sprayed NiCrAl coating containing inherited inter-splat boundaries, pores, and interfacial discontinuities to controlled ultrasonic impact treatment remains insufficiently understood.

The novelty of the present study lies in establishing the relationship between UNSM processing parameters and the competing processes of surface smoothing, mechanical modification, and damage accumulation in a detonation-sprayed NiCrAl coating. Unlike previous studies focusing mainly on bulk alloys or conventionally thermally sprayed coatings, the present work systematically evaluates the effects of both ultrasonic amplitude and normal load on phase-structural evolution, coating–substrate interface integrity, inter-splat and subsurface defects, mechanical response, friction behavior, and quantitative wear resistance.

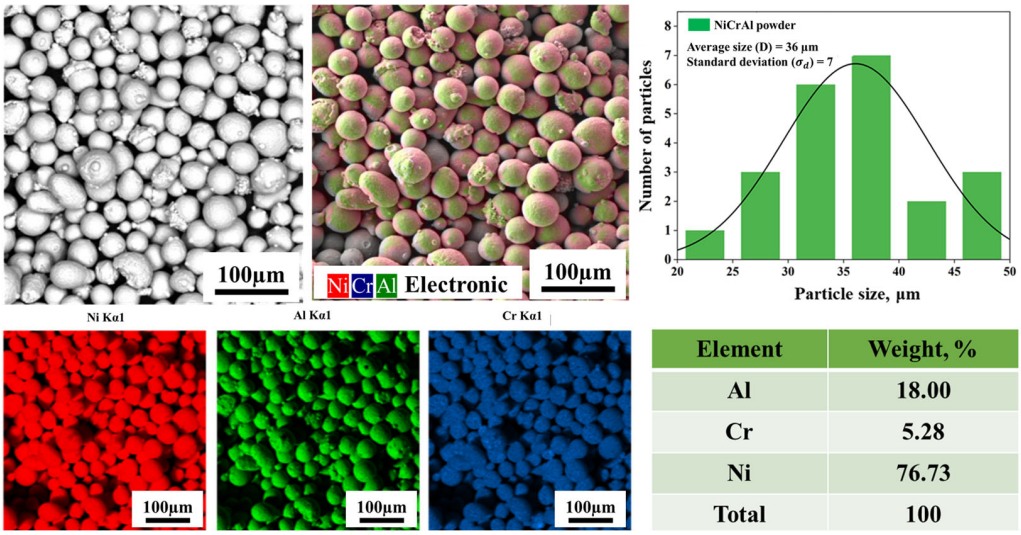
Therefore, the aim of this work is to systematically investigate the influence of ultrasonic vibration amplitude and normal load during UNSM on the phase-structural state, surface microgeometry, and mechanical and tribological properties of a detonation-sprayed NiCrAl coating, with particular attention to the evolution of inter-splat and subsurface defects and to the integrity of the coating–substrate interface.

2. Materials and Methods

For the deposition of NiCrAl coatings, 14MoV6-3 low-alloy steel, conforming to ISO 4955 [33], was used as the substrate material. The steel was machined into disc-shaped specimens with a diameter of 50 mm and a thickness of 3 mm. Prior to the coating process, the substrate surfaces were mechanically prepared by sequential grinding with abrasive SiC papers ranging from 120 to 2000 grit in order to remove surface contaminants, oxide layers,

and machining irregularities and to obtain a uniform surface condition. After grinding, the specimens were subjected to abrasive sandblasting treatment to increase the surface roughness and promote mechanical interlocking between the subsequently deposited coating and the steel substrate. This surface preparation procedure was employed to enhance the adhesion and interfacial bonding strength of the detonation-sprayed NiCrAl coating.

NiCrAl system powder was used as the starting material for the formation of detonation-sprayed coatings. The morphology, particle size distribution, and distribution of the main elements in the initial powder were investigated using scanning electron microscopy and energy-dispersive X-ray microanalysis (Figure 1). SEM images showed that the powder particles have predominantly spherical and near-spherical shapes with a relatively smooth surface. Along with individual particles, small agglomerates and particles with local surface irregularities are observed, which is characteristic of gas-atomized metallic powders. The particle size distribution of the initial NiCrAl powder was determined by image analysis of scanning electron microscopy (SEM) micrographs rather than by sieve analysis or laser diffraction. The analysis was performed in accordance with ASTM E2109 [34] using ImageJ software (version 1.54), in which the characteristic dimensions of individual powder particles were measured and used to construct the particle size distribution. The results showed that the particle sizes were predominantly in the range of approximately 20–50 μm. The average particle size was 36 μm, and the standard deviation was 7 μm. The majority of the particles are concentrated in the range of approximately 30–40 μm. The predominantly spherical morphology and relatively narrow particle size distribution provide good powder flowability, stable feeding into the barrel of the detonation spraying system, and relatively uniform interaction of the particles with the detonation products during spraying. Energy-dispersive analysis confirmed the presence of the main components Ni, Al, and Cr in the powder. The average elemental composition was 76.73 wt.% Ni, 18.00 wt.% Al, and 5.28 wt.% Cr. The elemental distribution maps show that Ni, Al, and Cr are present over the entire surface of the investigated particles without pronounced macroscopic segregation. Such a relatively uniform distribution of the components is an important prerequisite for the formation of a Ni–Al–Cr-containing coating structure during subsequent detonation spraying.



Element	Weight, %
Al	18.00
Cr	5.28
Ni	76.73
Total	100

Figure 1. The morphology, particle size distribution, and distribution of the main elements in the initial powder.

The NiCrAl coating was deposited using a CCDS2000 computer-controlled detonation spraying system, which enables precise regulation and reproducibility of the main tech-

nological parameters of the coating process [10,11,35]. The system was equipped with a straight cylindrical barrel with an internal diameter of 20 mm and an approximate length of 800 mm. The NiCrAl powder was introduced into the barrel through the powder-feeding port using nitrogen as the carrier gas and was subsequently accelerated by the detonation products toward the barrel outlet. The spraying distance between the barrel muzzle and the substrate surface was maintained at 150 mm. An oxygen–acetylene (O_2/C_2H_2) gas mixture was employed as the detonating fuel because this combination is widely used for the detonation spraying of metallic and composite powder materials due to its high combustion temperature and ability to generate a high-velocity particle flow. Depending on the stoichiometric ratio and chemical composition of the explosive mixture, the thermal and chemical conditions inside the detonation barrel may promote interactions between individual components and phases of the sprayed particles [35]. The technological parameters used for detonation spraying of the NiCrAl coating are presented in Table 1.

Table 1. Technological parameters of the detonation spraying process for producing NiCrAl coatings.

Sample Name	O_2/C_2H_2	Barrel Filling Volume with Explosive Gas, %	Spray Distance, mm	Shot Numbers
NiCrAl coating	1.856	50	150	20

Ultrasonic nanocrystalline surface modification (UNSM) of the detonation-sprayed NiCrAl coatings was performed using a UNSM VM200S system manufactured by Designmecha Co., Ltd. (Asan, Republic of Korea) equipped with a program-controlled XYZ coordinate stage [14,36,37]. The UNSM method is based on repeated high-frequency impact of a spherical indenter on the treated surface and belongs to the methods of severe plastic deformation of the surface layer [14]. Ultrasonic vibrations generated by a piezoelectric transducer are transmitted through a booster and a horn to the working tool. At the same time, the indenter is subjected to both a specified static normal load and a dynamic component generated by ultrasonic vibrations. As a result of successive overlapping impacts, local plastic deformation of the near-surface layer of the coating occurs, accompanied by changes in its surface microrelief and defect state [14,36]. The general view of the ultrasonic nanocrystalline surface modification system and its operating principle are shown in Figure 2.

A spherical tungsten carbide (WC) tip with a diameter of 2.38 mm was used as the working tool. The treatment was carried out at a constant ultrasonic vibration frequency of 20 kHz. The linear travel speed of the tool relative to the surface was 2000 mm/min (33.3 mm/s), and the step between adjacent passes was 70 μm. The selected step ensured multiple overlaps of the indenter impact zones and uniform treatment of the entire investigated coating area.

To evaluate the effect of UNSM intensity, the ultrasonic vibration amplitude A and the static normal load F_n were selected as the principal variable parameters because both directly influence the magnitude of repeated contact loading and the extent of plastic deformation introduced into the near-surface region. In the first series of experiments, the normal load was maintained constant at 10 N, while the amplitude was sequentially varied from 10 to 40 μm. The A10F10, A20F10, A30F10, and A40F10 conditions were investigated, corresponding to amplitudes of 10, 20, 30, and 40 μm at F_N = 10 N. To separately evaluate the effect of the normal load, the A10F20 condition was used, in which the amplitude was maintained at 10 μm, while the load was increased to 20 N. The complete UNSM processing parameters used for each treatment condition are summarized in Table 2. The ultrasonic frequency, tool travel speed, and step between adjacent passes were maintained constant

at 20 kHz, 2000 mm/min, and 70 μm, respectively, whereas the ultrasonic amplitude and normal load were varied according to the experimental design.

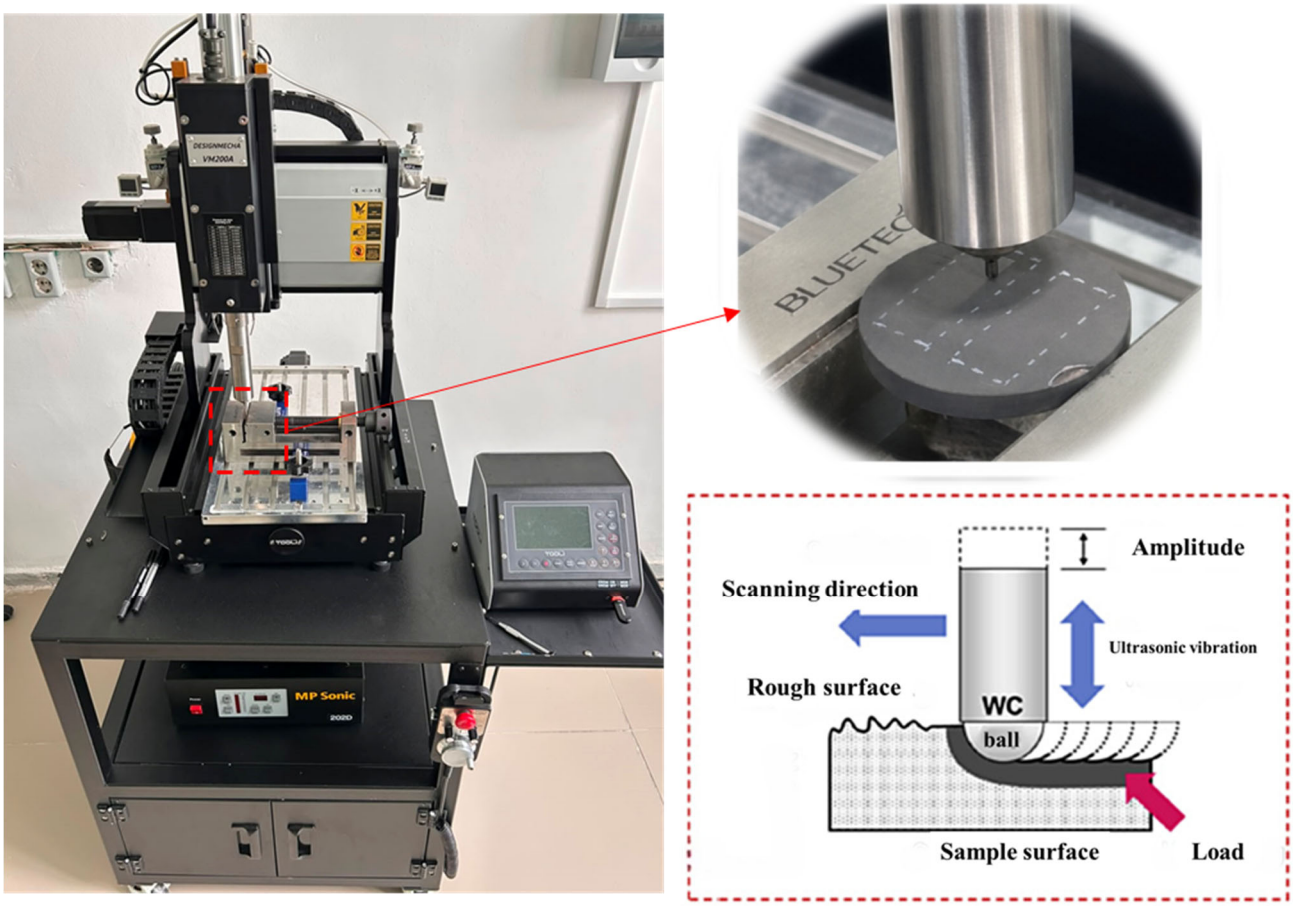


Figure 2. The general view of the ultrasonic nanocrystalline surface modification system and its operating principle.

Table 2. UNSM treatment parameters.

Sample Name	Amplitude A, μm	Normal Load F_N, N	Frequency, kHz	Treatment Speed, mm/min	Step Between Passes, μm
NiCrAl coating	-	-	-	-	-
A10F10	10	10	20	2000	70
A20F10	20	10	20	2000	70
A30F10	30	10	20	2000	70
A40F10	40	10	20	2000	70
A10F20	10	20	20	2000	70

The selection of the UNSM parameters was based on a combination of literature data, the operating characteristics of the UNSM system, and preliminary trials performed on the detonation-sprayed NiCrAl coating. A vibration frequency of 20 kHz was maintained constant because it corresponds to the nominal operating frequency of the UNSM system and is widely used in conventional UNSM treatment [14,36]. The tool travel speed of 2000 mm/min and the 70 μm step between adjacent passes were selected to provide stable processing and sufficient overlap between successive impact tracks, thereby ensuring treatment of the entire coating surface. The ultrasonic amplitude and static normal load were chosen as the main variable parameters because they directly control the intensity of repeated contact loading and, consequently, the degree of near-surface plastic deformation.

In the first series, the normal load was fixed at 10 N while the amplitude was increased stepwise from 10 to 40 μm, allowing the effect of increasing dynamic impact intensity to be evaluated. In the second series, the amplitude was fixed at 10 μm and the normal load was increased from 10 to 20 N to isolate the effect of static contact loading. The investigated range was additionally constrained by preliminary trials: further increases in amplitude and/or normal load caused local coating failure, chipping, and delamination from the substrate. Therefore, the selected A10F10–A40F10 and A10F20 conditions represent a practical processing window spanning moderate to intense UNSM treatment while preserving the macroscopic integrity of the detonation-sprayed NiCrAl coating during processing.

The phase composition and structural state of the investigated coatings were analyzed by X-ray diffraction (XRD) using a DX-27mini benchtop diffractometer manufactured by Dandong Haoyuan Instrument Co., Ltd. (Dandong, China). Prior to XRD measurements, no additional grinding or polishing of the coating surface was performed after UNSM treatment in order to preserve the mechanically modified near-surface layer. The diffractometer was equipped with a copper-anode X-ray tube operated at an accelerating voltage of 40 kV and a current of 30 mA. Diffraction patterns were recorded using Cu-Kα radiation with a wavelength of $\lambda = 1.541$ Å over the angular range $2\theta = 20–90^{\circ}$. The scanning step was set to 0.02°, with a counting time of 0.5 s per step. Phase identification and interpretation of the diffraction peaks were performed using HighScore software (v3.0e(3.0.5), Malvern Panalytical, Almelo, The Netherlands) in combination with the PDF-2 crystallographic database.

The microstructural features, surface morphology, and cross-sectional architecture of the coatings were examined by scanning electron microscopy (SEM) using an SEM3200 microscope (CIQTEK, Hefei, China). Local elemental composition and spatial distribution of the principal chemical elements were additionally investigated by energy-dispersive X-ray spectroscopy (EDS/EDX) using a Bruker analytical system (Bruker Nano GmbH, Berlin, Germany). For quantitative evaluation of compositional changes associated with detonation spraying, EDS point analyses were additionally performed at five representative locations on the surface of the as-sprayed NiCrAl coating. The elemental concentrations were reported as normalized mass fractions, and the mean values and standard deviations were calculated from the five measurements. For direct comparison with the nominal metallic composition of the initial powder, the Ni, Al, and Cr contents of the coating were additionally normalized excluding carbon from the compositional balance. Cross-sectional SEM observations were used to evaluate coating continuity, interfacial morphology, pores, microdefects, and structural heterogeneity, while elemental line scans and mapping were employed to characterize the distribution of Ni, Cr, Al, Fe, and other detected elements across the coating–substrate system.

The tribological behavior of the coatings was evaluated under dry sliding conditions using the ball-on-disk configuration on a TRB3 tribometer (Anton Paar GmbH, Graz, Austria) in accordance with ASTM G99 [38]. A 3.0 mm diameter SH15 steel ball was used as the counterbody. The tests were performed under a normal load of 10 N at a linear sliding velocity of 0.03 m/s over a total sliding distance of 100 m. During testing, the coefficient of friction was continuously recorded as a function of sliding distance. For each coating condition, one tribological test was performed under identical testing conditions. Therefore, the friction curves represent individual experimental runs and are not presented with statistical error bars. The tribological response was additionally evaluated by profilometric analysis of the wear tracks and SEM/EDS examination of the worn surfaces in order to provide complementary evidence for the observed wear behavior. After the tribological tests, the wear-track profiles were measured using a profilometer in accordance with ISO 13565 [39]. In addition to profilometric measurements,

the morphology and elemental composition of the wear tracks after tribological testing were examined by scanning electron microscopy in backscattered-electron mode and by energy-dispersive X-ray spectroscopy using the same SEM/EDS system described above. SEM observations were used to identify local plastic deformation, cracking, delamination, debris accumulation, and material pull-out within the wear scars, while EDS elemental mapping was employed to evaluate elemental redistribution and possible transfer of material within the tribological contact. The cross-sectional area of the wear track (S) was determined from the measured transverse profiles and used as a quantitative parameter for comparing the relative wear resistance of the coatings under different UNSM treatment conditions. The wear-track width and maximum depth were not separately quantified in the present study. Therefore, the cross-sectional area was used as an integral geometrical parameter of the transverse wear profile, while the wear mechanism was interpreted in combination with the SEM/EDS observations of the worn surfaces. Since one tribological test was performed for each condition, the reported wear-track cross-sectional areas are presented as individual measured values rather than statistically averaged data. The wear-track profiles and corresponding cross-sectional areas were processed using InstrumX 8.1.10 software integrated with the TRB3 tribometer system. This combined approach enabled correlation of the coating roughness, mechanical properties, phase composition, microstructure, friction behavior, and wear resistance.

Instrumented hardness measurements were performed on the top surface of the as-sprayed and UNSM-treated NiCrAl coatings using a FISCHERSCOPE HM2000 instrumented indentation tester (Helmut Fischer GmbH, Sindelfingen, Germany). A maximum load of 1000 mN was applied during each measurement. For each coating condition, five independent indentations (n = 5) were performed at different locations on the coating surface, with sufficient spacing between adjacent indents to minimize mutual interaction. The hardness and elastic modulus are reported as the arithmetic mean ± standard deviation (SD). Numerical results are reported with a precision consistent with the corresponding standard deviation, with mean values and standard deviations rounded to the same decimal place. Considering the heterogeneous lamellar and multiphase structure of the detonation-sprayed coating, the measured values are interpreted as local instrumented indentation hardness rather than as a spatially homogeneous bulk hardness. All indentations were performed normal to the top surface of the coating within the UNSM-treated area. However, the penetration depth of the indenter and the thickness of the UNSM-modified layer were not independently quantified in the present study. Therefore, the measured hardness values should be interpreted as the local indentation response of the near-surface coating region sampled by the indenter, rather than as a property attributable exclusively to the mechanically modified layer. The SD was used to quantify the scatter in the indentation response associated with the intrinsically heterogeneous lamellar and multiphase structure of the detonation-sprayed coating.

3. Results and Discussion

3.1. Roughness

After UNSM treatment, the average roughness of the detonation-sprayed NiCrAl coating decreased significantly compared with the initial value (Ra = 3.78 μm). For the A10F10 and A20F10 conditions, identical average values (Ra = 2.40 μm) were obtained, corresponding to a reduction of approximately 36.5%. Further increasing the ultrasonic amplitude to 30 μm at a constant normal load of 10 N (A30F10) reduced Ra to 1.94 μm, whereas the A40F10 condition resulted in a sharp decrease in roughness to 0.25 μm, i.e., by approximately 93.4% compared with the initial state. This pronounced surface smoothing should not be interpreted as evidence of improved subsurface structural integrity, since

UNSM may simultaneously flatten the outermost asperities and activate inherited defects beneath the surface. Under the A10F20 condition, Ra also decreased significantly to 0.81 μm, indicating a substantial influence of the load parameter: increasing the normal load enhances the intensity of contact plastic deformation and the efficiency of surface smoothing. It should also be noted that further increases in load or amplitude beyond the selected conditions led to local delamination or failure of the NiCrAl coating. This indicates the existence of a critical technological range of UNSM intensity [25–27]. It should be noted that the present roughness assessment is based on Ra values; therefore, additional parameters such as Rz and Rmax, as well as full surface-profile analysis, would be useful for a more detailed characterization of the peak-to-valley topography in future studies.

3.2. Phase Composition

The results of X-ray phase analysis of the detonation-sprayed NiCrAl coatings in the as-sprayed state and after UNSM treatment are presented in Figure 3. X-ray phase analysis of the as-sprayed NiCrAl coating revealed the presence of the AlNi and Al_4Ni_3 intermetallic phases, as well as the $AlCr_2$ phase. In the X-ray diffraction pattern of the as-sprayed coating, the intense, relatively narrow AlNi(110) reflection dominates, whereas the AlNi(100), AlNi(211), Al_4Ni_3(444), and $AlCr_2$(202) reflections exhibit significantly lower intensities. The formation of Ni–Al phases is characteristic of detonation spraying of the Ni–Cr–Al system and strongly depends on the energy parameters of the spraying process. Rakhadilov et al. also established the formation of Ni–Al-containing phases in detonation-sprayed Ni–Cr–Al coatings under different spraying conditions [10].

After UNSM, pronounced broadening of the diffraction peak in the $AlCr_2$(103)/AlNi(110) region and a decrease in its maximum intensity compared with the as-sprayed coating were observed under all investigated conditions. Changing the UNSM amplitude at a constant load of F10 significantly affects the diffraction pattern of the coating. Already after A10F10, the narrow AlNi(110) reflection of the as-sprayed coating transforms into a broad $AlCr_2$(103)/AlNi(110) peak, indicating that the A10F10 condition provides sufficient impact intensity for pronounced plastic modification of the surface layer. With a further increase in amplitude to A20 and A30, the overall set of the main AlNi–Al_4Ni_3–$AlCr_2$ phases is retained; however, the relative prominence of the weak Al_4Ni_3 reflections changes. The most pronounced change in the phase-diffraction state was observed after the A40F10 condition. In addition to AlNi, Al_4Ni_3, and $AlCr_2$, additional weak Al_3Ni_5 reflections were indexed in the X-ray diffraction pattern for this condition. Their appearance may be associated with deformation-induced redistribution of the phase state of the Ni–Al system due to the higher intensity of cyclic impact loading. The possibility of phase transformations during UNSM is confirmed by experimental studies of other metallic systems: Polonyankin et al. showed by XRD that the accumulation of deformation energy during UNSM can lead to systematic changes in the phase composition of the surface layer [40].

Comparison of A10F10 and A10F20 makes it possible to evaluate the effect of increasing the load at a constant amplitude. Both states are characterized by a similar set of phases and pronounced broadening of the main $AlCr_2$(103)/AlNi(110) peak, whereas no qualitatively new reflections are observed for A10F20. This indicates that increasing the load from F10 to F20 at A10 alters the degree and depth of the plastically deformed state to a greater extent than the principal phase composition of the coating.

An additional consideration in interpreting the XRD results is the relationship between the X-ray information depth and the thickness of the mechanically modified layer produced by UNSM. In conventional symmetric θ–2θ geometry, the effective X-ray penetration depth is not constant but depends on the diffraction angle and the linear absorption coefficient of the material; for the 1/e attenuation criterion, it can be approximated as $t\propto = \sin\theta/(2\mu)$.

Since the exact depth of the plastically modified layer was not independently measured in the present study, it cannot be unequivocally established whether the X-ray information depth was smaller or larger than the UNSM-affected depth. Therefore, the diffraction patterns should be interpreted as a depth-averaged structural response that may contain contributions from both the strongly deformed near-surface region and the deeper, less-deformed coating material. Consequently, the observed peak broadening, intensity redistribution, and changes in peak shape are consistent with deformation-induced structural modification of the UNSM-affected region; however, their magnitude may be partially attenuated by diffraction from the underlying material. The conventional θ–2θ measurements used in this study therefore cannot provide a quantitative determination of the depth of the UNSM-modified zone. Depth-resolved techniques, such as grazing-incidence X-ray diffraction (GIXRD), cross-sectional EBSD, or TEM, would be required to quantitatively characterize the structural gradient produced by UNSM.

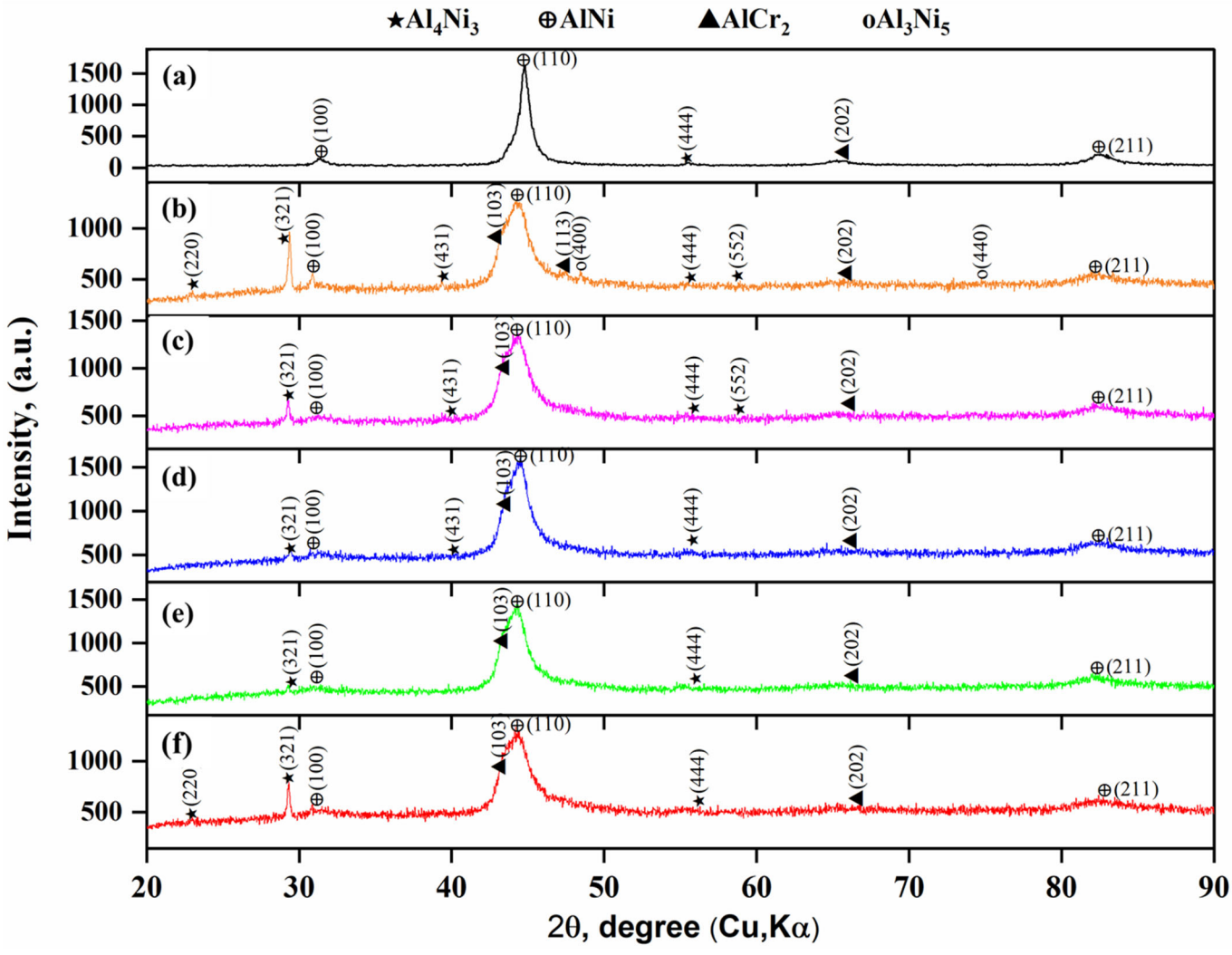


Figure 3. The results of X-ray phase analysis of the detonation-sprayed NiCrAl coatings in the as-sprayed state (**a**) and after UNSM treatment: (**b**) A10F10; (**c**) A20F10; (**d**) A30F10; (**e**) A40F10; (**f**) A10F20.

3.3. Microstructure: Elemental Distribution

Figure 4 compares the cross-sectional microstructure of the detonation-sprayed NiCrAl coating in the as-sprayed state and after UNSM treatment under all investigated conditions. The as-sprayed coating exhibits a relatively dense and continuous lamellar structure with

a characteristic wavy coating–substrate interface. Local pores, inter-splat discontinuities, and isolated interfacial defects are present within the coating, reflecting the heterogeneous particle-by-particle deposition mechanism of detonation spraying. No extensive delamination of the coating from the substrate is observed. After A10F10 treatment, the coating remains macroscopically continuous and well bonded to the substrate. The inherited pores and inter-splat discontinuities are still visible, but their opening remains relatively limited. Increasing the ultrasonic amplitude to 20 μm at the same normal load (A20F10) produces a more pronounced mechanical modification of the lamellar structure. Elongated discontinuities oriented approximately parallel to the coating surface become more evident, indicating progressive activation of pre-existing inter-splat boundaries. For the A30F10 condition, the coating continues to retain overall continuity and adhesion to the substrate, while local opening of inter-splat and subsurface defects becomes more noticeable. These defects are mainly elongated and follow the lamellar architecture of the deposited layer. At the same time, no large-scale delamination is observed in the examined cross-sections. Thus, A30F10 represents an intermediate condition in which substantial mechanical modification of the coating is achieved while macroscopic structural integrity is preserved. A further increase in the ultrasonic amplitude to 40 μm (A40F10) results in more pronounced defect opening within the coating. Elongated crack-like discontinuities and local subsurface defects are more clearly developed than under the lower-amplitude conditions. A similar trend is observed for A10F20, where the ultrasonic amplitude is maintained at 10 μm but the normal load is increased to 20 N. In this case, the higher static load promotes the opening of structurally weak regions within the lamellar coating, including elongated internal and near-surface discontinuities. Comparison of A10F10 and A10F20 therefore demonstrates that increasing the normal load alone can substantially intensify local contact stresses and activate inherited defects, even without increasing the vibration amplitude. Overall, the SEM observations reveal a progressive evolution from relatively localized inherited defects in the as-sprayed and low-intensity UNSM conditions toward more pronounced inter-splat and subsurface defect opening at higher treatment intensity. Importantly, the observed changes should not be interpreted as the formation of entirely new defects under UNSM. Rather, the treatment progressively activates and opens pre-existing structural discontinuities inherent to the lamellar detonation-sprayed coating. This behavior is consistent with the concept of a limited processing window in which beneficial surface deformation and compaction compete with damage accumulation within mechanically weak inter-splat regions.

The EDS line-scan profiles for all investigated conditions are compared in Figure 5. In the as-sprayed coating, Ni, Al, and Cr are the dominant elements throughout the coating thickness, whereas the Fe signal remains low until the coating–substrate interface is reached. At a depth of approximately 75–90 μm, depending on the analyzed cross-section, the Ni, Al, and Cr signals decrease sharply while the Fe signal simultaneously increases, indicating a relatively distinct chemical boundary between the NiCrAl coating and the steel substrate. A similar elemental-transition pattern is retained after all UNSM treatments. Neither increasing the ultrasonic amplitude from 10 to 40 μm nor increasing the normal load from 10 to 20 N produces an extended compositional transition zone across the interface. The principal coating elements remain concentrated within the NiCrAl layer, while Fe remains predominantly localized in the substrate. These results indicate that the structural changes observed by SEM after UNSM are primarily associated with mechanical deformation, compaction, and defect evolution rather than with large-scale chemical mixing or diffusional redistribution across the coating–substrate interface.

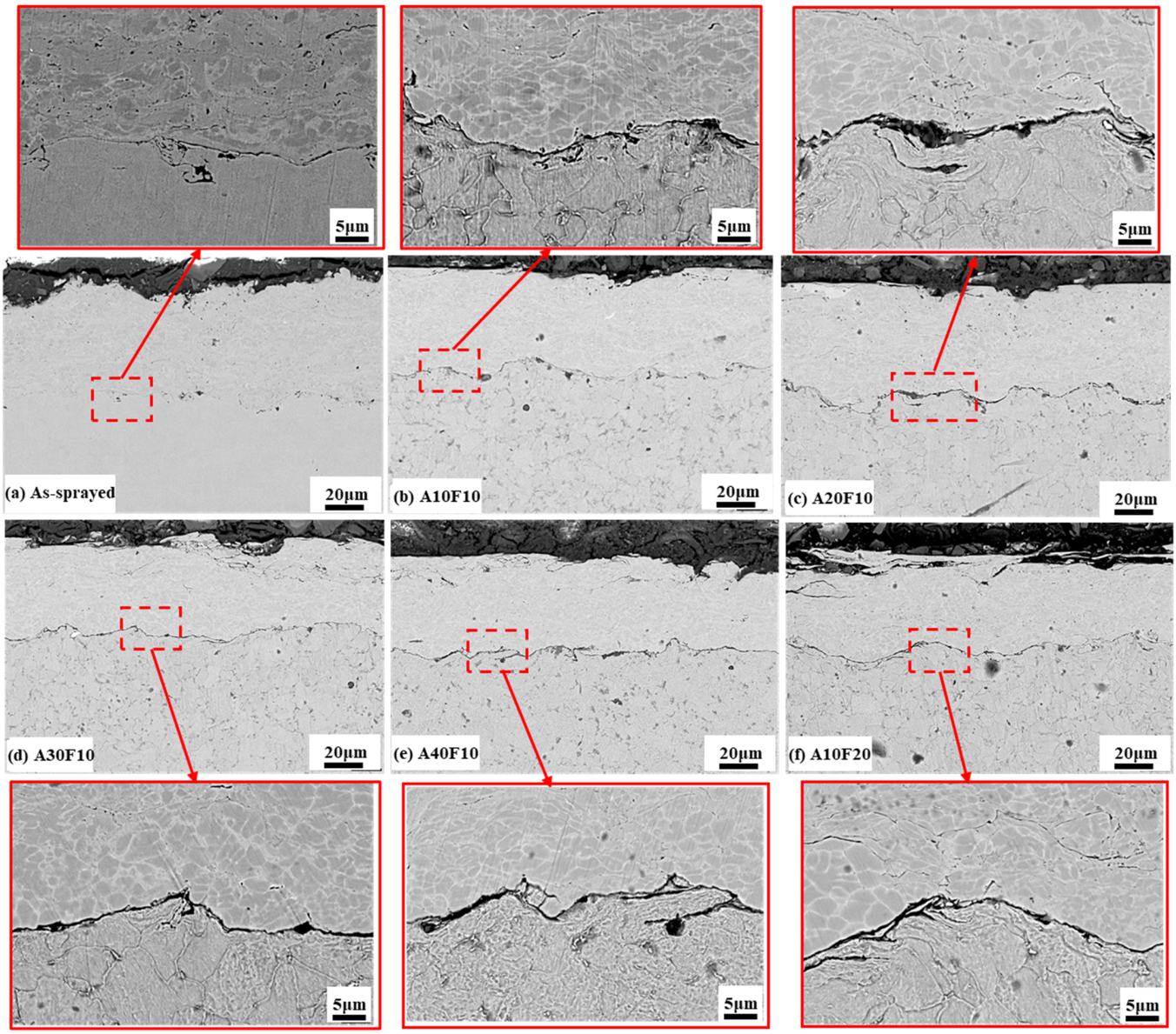


Figure 4. Cross-sectional SEM/BSE images showing the microstructural evolution of the detonation-sprayed NiCrAl coating: (**a**) as-sprayed; (**b**) A10F10; (**c**) A20F10; (**d**) A30F10; (**e**) A40F10; and (**f**) A10F20. The enlarged images highlight representative inter-splat, subsurface, and coating–substrate interfacial discontinuities.

Quantitative EDS point analysis of the as-sprayed NiCrAl coating was performed at five representative surface locations. The mean normalized mass concentrations were 73.04 ± 0.29 wt.% Ni, 19.07 ± 1.84 wt.% Al, 4.50 ± 1.76 wt.% Cr, and 3.39 ± 0.28 wt.% C. The Al concentration varied from 16.69 to 20.71 wt.%, reflecting the local compositional heterogeneity of the detonation-sprayed coating. After excluding carbon and renormalizing the metallic constituents to the sum Ni + Al + Cr, the coating composition corresponded to approximately 75.60 wt.% Ni, 19.74 wt.% Al, and 4.66 wt.% Cr. For comparison, the initial powder contained 76.73 wt.% Ni, 18.00 wt.% Al, and 5.28 wt.% Cr. Therefore, no measurable depletion of Al was detected after detonation spraying within the accuracy and limitations of the present EDS analysis. Since oxygen was not included in the quantitative point analysis, preferential Al oxidation during spraying cannot be directly quantified from these measurements.

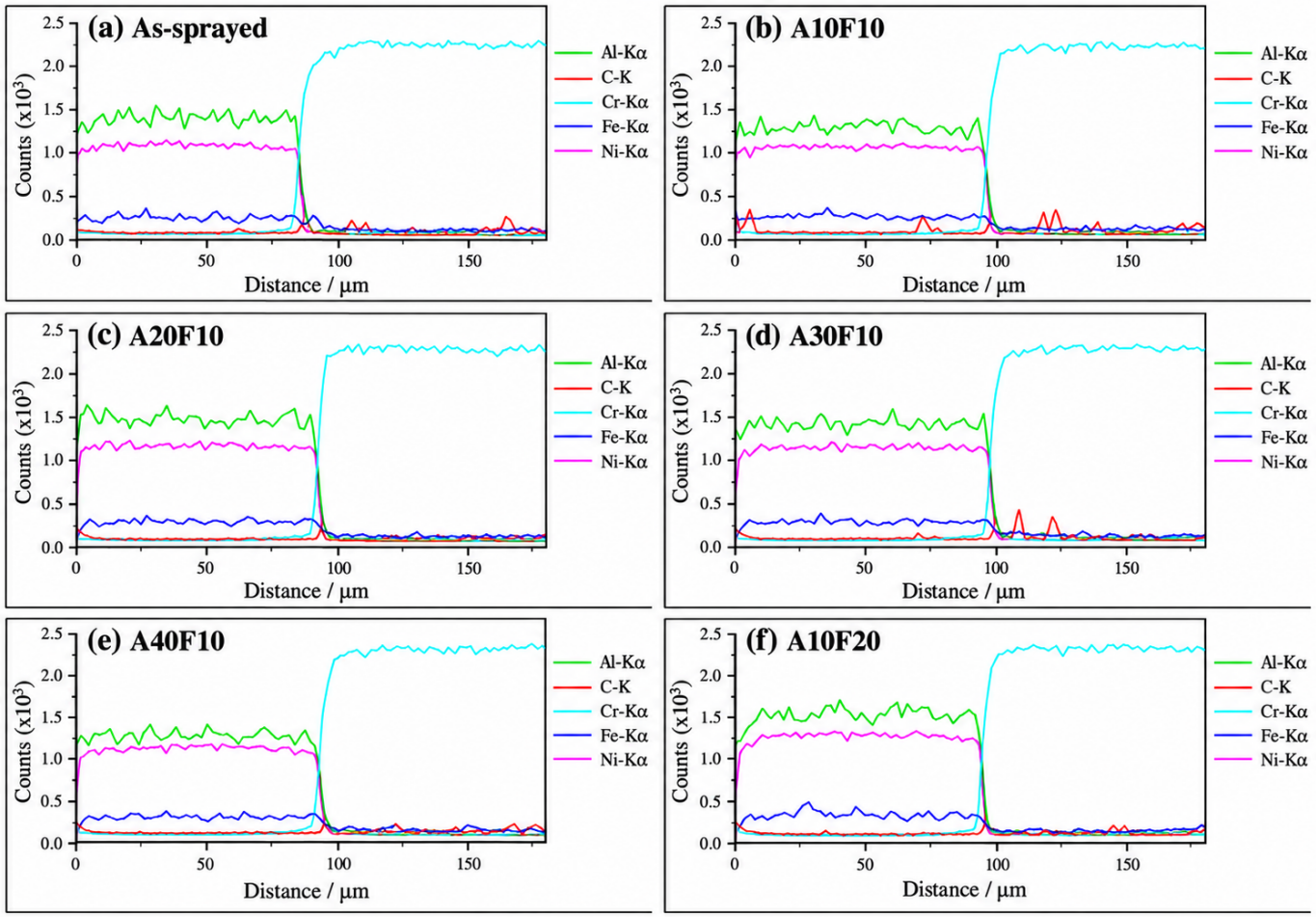


Figure 5. EDS line-scan profiles across the NiCrAl coating–steel substrate interface: (**a**) as-sprayed; (**b**) A10F10; (**c**) A20F10; (**d**) A30F10; (**e**) A40F10; and (**f**) A10F20.

The elemental distribution maps presented in Figures 6 and 7 are consistent with the line-scan results. In all investigated conditions, Ni, Al, and Cr are predominantly localized within the coating, whereas Fe is concentrated in the steel substrate. The elemental boundary closely follows the wavy morphology of the coating–substrate interface. No large regions of depletion of the principal NiCrAl constituents or extensive Fe penetration into the coating are observed after UNSM. The similarity of the elemental distribution patterns before and after treatment confirms that the increasing prominence of inter-splat and subsurface defects at A30F10, A40F10, and A10F20 is not associated with macroscopic chemical segregation. Instead, these structural features are attributed mainly to the mechanical response of the heterogeneous lamellar coating to repeated ultrasonic impact loading. Local oxygen and carbon signals are also detected in the maps; however, the high C and O intensities observed directly above the outer coating boundary are most likely associated with materials used during metallographic preparation and should not be interpreted as evidence of a thick surface oxide layer.

Taken together, the SEM and EDS results demonstrate that UNSM primarily modifies the mechanical and defect state of the detonation-sprayed NiCrAl coating while preserving the overall chemical separation between the coating and the steel substrate. The evolution of the microstructure depends strongly on treatment intensity: moderate conditions promote substantial deformation and local compaction while maintaining macroscopic coating integrity, whereas excessive ultrasonic amplitude or normal load progressively activates inherited inter-splat and subsurface discontinuities. This microstructural evolution pro-

vides an important basis for interpreting the non-monotonic mechanical response and the tribological behavior discussed in the following sections.

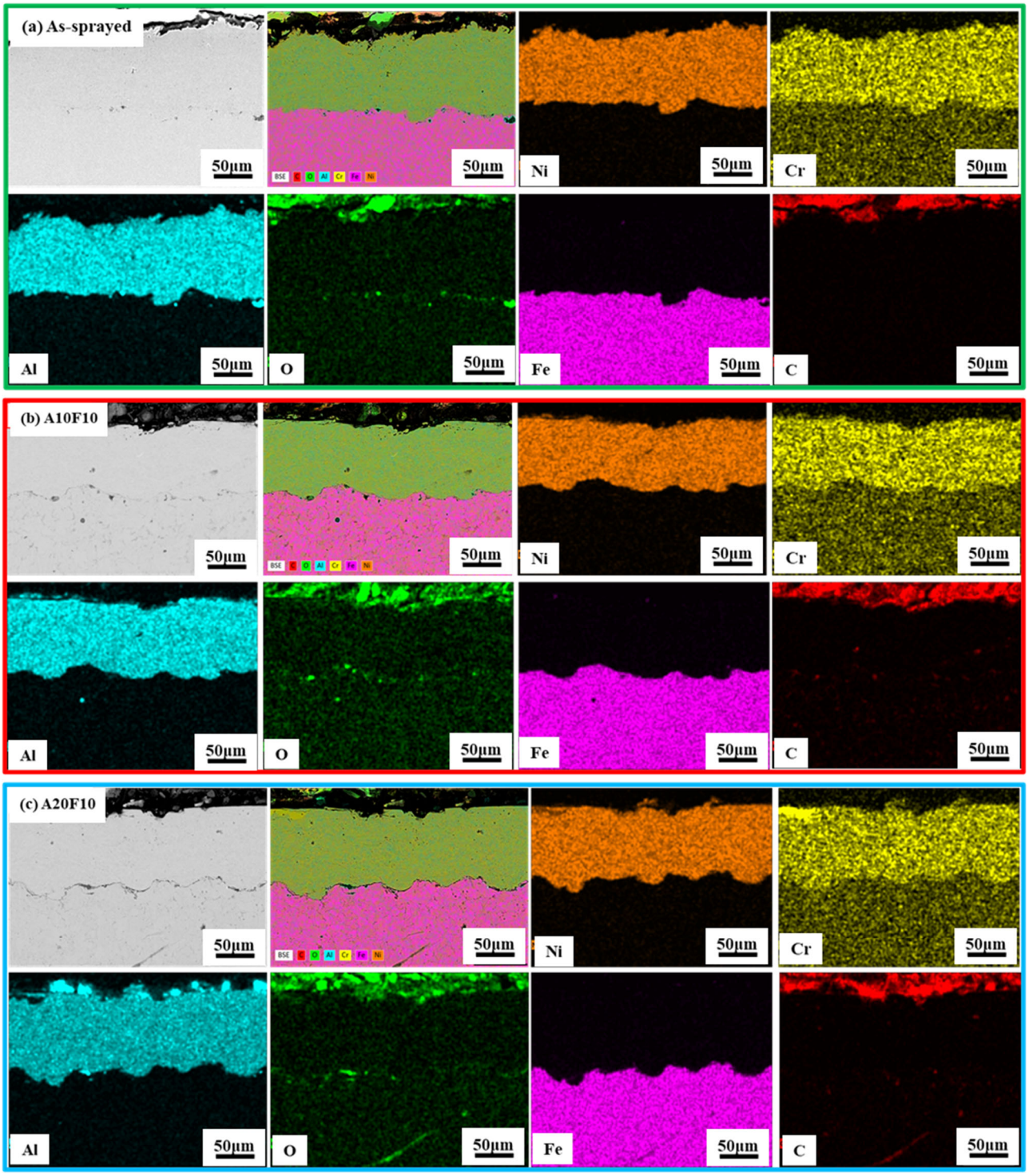


Figure 6. BSE images and EDS elemental distribution maps of the detonation-sprayed NiCrAl coating (**a**) as-sprayed and after UNSM treatment: (**b**) A10F10; (**c**) A20F10.

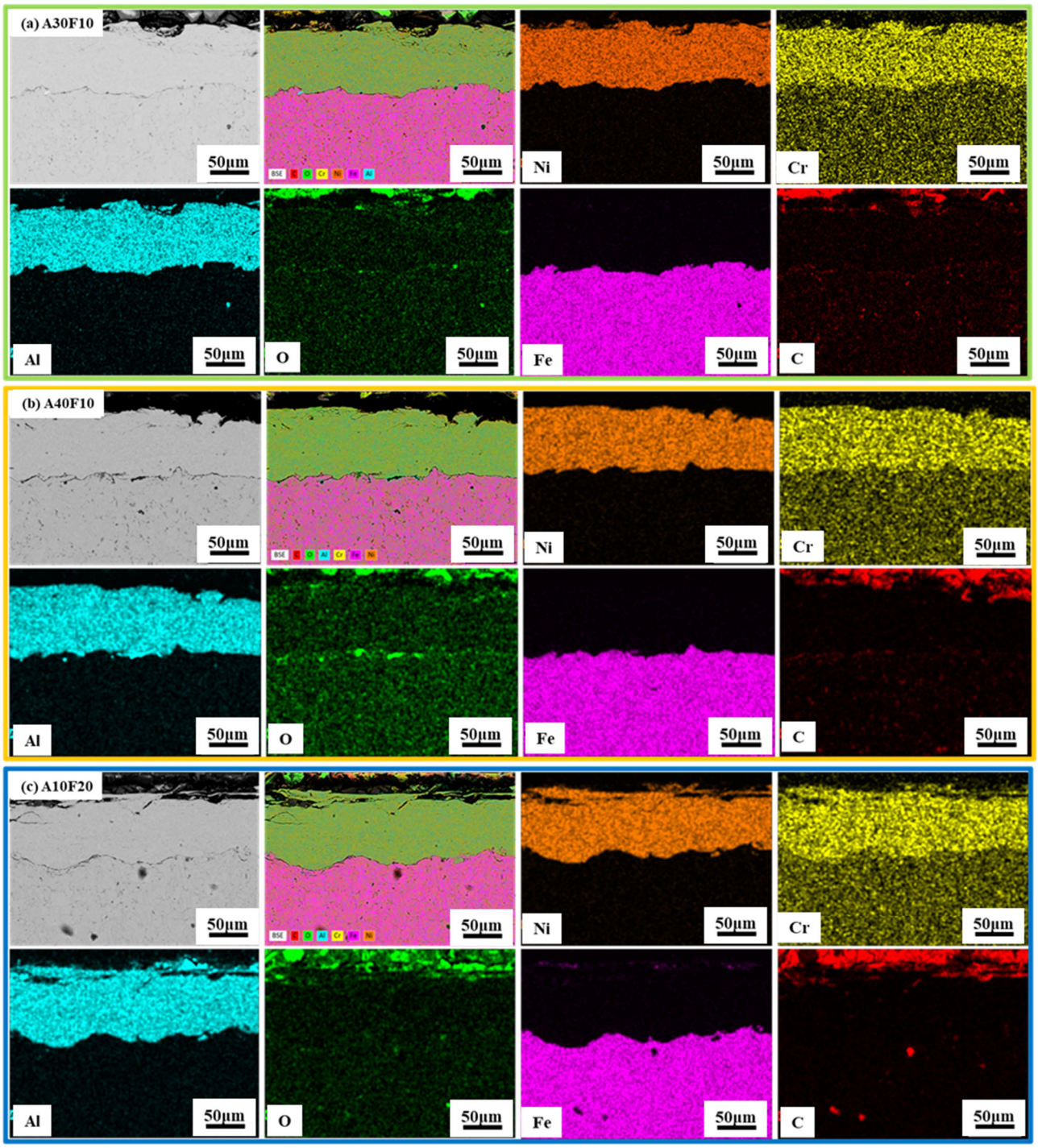
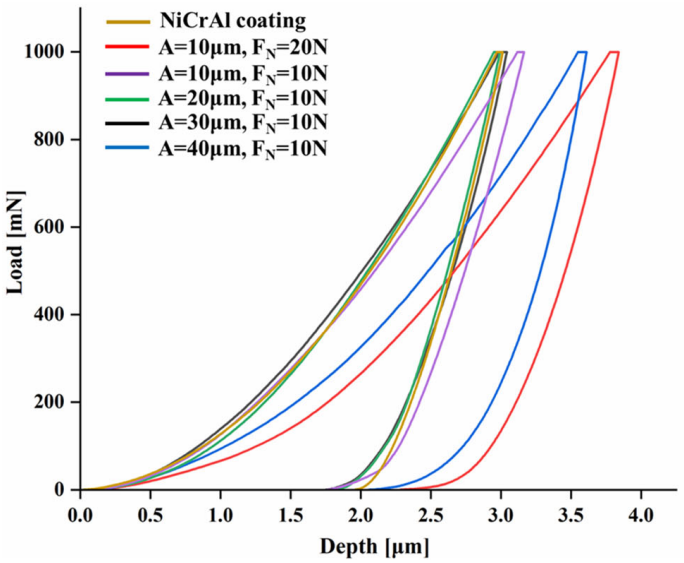


Figure 7. BSE images and EDS elemental distribution maps of the detonation-sprayed NiCrAl coating after UNSM treatment: (**a**) A30F10; (**b**) A40F10; and (**c**) A10F20.

3.4. Microhardness

The microhardness and elastic modulus results (mean ± SD, n = 5) showed a non-monotonic effect of the UNSM parameters on the mechanical properties of the detonation-sprayed NiCrAl coating (Figure 8). The as-sprayed coating exhibited an average hardness of 623 ± 77 HV. After treatment at A10F10, the average hardness was 607 ± 101 HV, which is comparable to the as-sprayed value. For A20F10 and A30F10, the mean hardness values were 660 ± 95 and 656 ± 189 HV, respectively. Although these mean values are slightly higher than that of the as-sprayed coating, the differences are small relative to the cor-

responding standard deviations. Therefore, the present measurements do not provide sufficient statistical evidence to claim a significant increase in hardness for the A20F10 and A30F10 conditions. Instead, these states should be regarded as retaining a hardness level comparable to that of the as-sprayed coating, albeit with substantial local scatter associated with the heterogeneous lamellar microstructure. In contrast, the A40F10 and A10F20 conditions exhibited markedly lower mean hardness values of 397 ± 98 and 381 ± 139 HV, respectively. The pronounced reduction in the mean hardness under these more severe treatment conditions is consistent with the SEM observations showing increased opening of inherited inter-splat and subsurface discontinuities. The simultaneous decrease in surface roughness and reduction in hardness under the A40F10 condition are not contradictory because these measurements characterize different aspects and potentially different depth ranges of the coating response. The very low Ra value primarily reflects the geometrical state of the outer surface, where intense repeated impacts promote plastic flattening of asperities. In contrast, instrumented indentation samples a finite volume beneath the contact surface and may therefore be influenced by the underlying heterogeneous lamellar structure, including inter-splat and subsurface discontinuities. Since neither the maximum indentation depth nor the thickness of the UNSM-modified layer was independently quantified, the measured hardness cannot be attributed exclusively to the outermost smoothed layer. Thus, severe UNSM may produce pronounced surface smoothing while simultaneously activating mechanically weak subsurface regions that reduce the local load-bearing response measured by indentation. The results therefore indicate that moderate UNSM conditions do not produce a statistically demonstrable hardening of the coating, whereas more severe treatment conditions are associated with a pronounced reduction in the local indentation hardness.



Samples	HV	E, GPa
NiCrAl coating	623 ± 77	121 ± 12
A=10μm F$_N$=20N	381 ± 139	92 ± 14
A=10μm F$_N$=10N	607 ± 101	101 ± 14
A=20μm F$_N$=10N	660 ± 95	124 ± 24
A=30μm F$_N$=10N	656 ± 189	122 ± 37
A=40μm F$_N$=10N	397 ± 98	120 ± 33

Figure 8. Microhardness and elastic modulus of the detonation-sprayed NiCrAl coatings before and after UNSM treatment.

The present results are generally consistent with recent studies showing that UNSM can improve the mechanical response of thermally sprayed coatings through plastic deformation, surface compaction, and microstructural refinement. Amanov and Berkebile reported that UNSM treatment of HVOF-sprayed Cr_2O_3 and Cr_3C_2–NiCr coatings reduced surface roughness and increased surface hardness [25]. However, unlike the predominantly beneficial response reported for these coatings, the present detonation-sprayed NiCrAl coating exhibits a clearly non-monotonic mechanical response: the moderate A20F10 and

A30F10 conditions retain hardness values comparable to that of the as-sprayed coating within the experimental scatter, whereas the more severe A40F10 and A10F20 conditions result in pronounced hardness reduction. This difference is attributed to the activation and opening of inherited inter-splat and subsurface defects when the imposed cyclic impact intensity exceeds the load-bearing capability of the lamellar coating structure.

The relatively large standard deviations observed for hardness and elastic modulus are associated with the heterogeneous nature of the detonation-sprayed NiCrAl coating. In addition, the multiphase AlNi–Al_4Ni_3–$AlCr_2$-based structure identified by XRD may contribute to local variations in the indentation response. Thus, the observed standard deviations reflect not only experimental scatter but also the intrinsic structural heterogeneity of the detonation-sprayed and subsequently mechanically modified coating. Unlike a homogeneous bulk material, the coating consists of plastically deformed splats separated by inter-splat boundaries and contains local pores, microvoids, and structurally non-uniform regions. Therefore, individual indentations may interact with areas having different local load-bearing capacities, which results in noticeable scatter in the measured mechanical properties. This effect becomes more pronounced for the A30F10, A40F10, and A10F20 conditions, where SEM observations revealed local inter-splat discontinuities and subsurface defects.

For the A20F10, A30F10, and A40F10 conditions, the mean elastic modulus values were 124 ± 24, 122 ± 37, and 120 ± 33 GPa, respectively, compared with 121 ± 12 GPa for the as-sprayed coating. Considering the magnitude of the corresponding standard deviations, these differences are within the experimental scatter and do not provide sufficient evidence of a systematic change in elastic modulus under these treatment conditions. In contrast, the A10F20 condition exhibited a markedly lower mean elastic modulus of 92 ± 14 GPa, corresponding to an approximately 24% reduction relative to the as-sprayed coating. This decrease indicates a substantial reduction in the local elastic stiffness of the coating under the higher normal load. Together with the decrease in hardness to 381 ± 139 HV and the inter-splat and subsurface discontinuities observed by SEM, this result suggests a deterioration of the local structural integrity and load-bearing response of the coating. However, because interfacial adhesion strength was not independently measured after UNSM treatment, the decrease in elastic modulus should not be interpreted as direct quantitative evidence of a loss of coating–substrate adhesion.

3.5. Tribological Behavior and Wear Mechanism

The results of tribological tests showed that ultrasonic nanocrystal surface modification has a non-monotonic effect on the friction behavior of the detonation-sprayed NiCrAl coating (Figure 9). The as-sprayed coating exhibited the lowest and most stable coefficient of friction. After the running-in stage, the coefficient of friction reached approximately 0.39–0.40 and remained nearly constant until the end of the test. In contrast, all UNSM-treated coatings exhibited higher friction coefficients during the initial stage of sliding, reaching approximately 0.78–0.80. Thus, the reduction in surface roughness after UNSM was not accompanied by a corresponding reduction in friction. For the A10F10 condition, the coefficient of friction stabilized at approximately 0.70–0.75 after the initial increase, with noticeable fluctuations during the subsequent sliding stage. The A10F20 condition also exhibited an increased coefficient of friction, which gradually decreased to approximately 0.68–0.70. The highest and most persistent friction level was observed for A20F10, where the coefficient remained at approximately 0.78–0.83 during most of the test. In contrast, A30F10 showed the most favorable evolution among the UNSM-treated conditions: after reaching approximately 0.80 during the initial stage, the coefficient of friction gradually decreased and reached approximately 0.53–0.55 toward the end of the test. For A40F10,

the coefficient initially decreased during sliding but increased sharply at the later stage, indicating instability of the tribological contact. Since one tribological test was performed for each coating condition, the friction curves are interpreted as comparative experimental trends rather than statistically averaged responses. The present friction behavior differs from that reported for several other UNSM-treated thermally sprayed coatings, where simultaneous reductions in friction and wear have been observed [27–29]. In the present detonation-sprayed NiCrAl coating, however, the coefficient of friction increased after UNSM while the amount of material removal decreased considerably. This indicates that the tribological response cannot be described solely in terms of initial surface roughness or friction coefficient and must instead be considered together with the mechanically modified state of the coating, inter-splat integrity, defect evolution, and the stability of the wear contact.

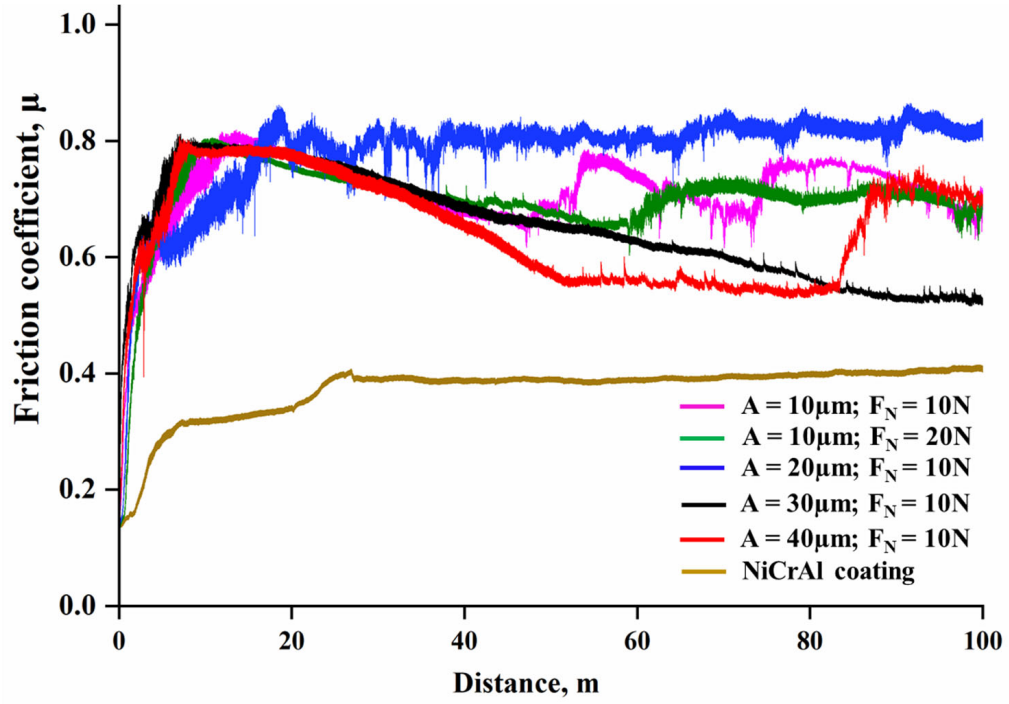


Figure 9. Coefficient of friction of the detonation-sprayed NiCrAl coatings before and after UNSM treatment.

Profilometric analysis confirmed a pronounced decrease in the wear-track cross-sectional area after most UNSM treatments (Figure 10). The as-sprayed coating exhibited the largest wear-track cross-sectional area of 7570 μm^2. After A10F10 and A20F10 treatments, the area decreased to 2637 and 2322 μm^2, corresponding to reductions of approximately 65.2% and 69.3%, respectively. The minimum value of 1425 μm^2 was obtained for A30F10, representing an approximately 81.2% reduction compared with the as-sprayed coating. For A10F20, the wear-track cross-sectional area was 1631 μm^2, corresponding to a reduction of approximately 78.5%. In contrast, A40F10 exhibited a substantially larger wear-track area of 6063 μm^2. Although this value remained approximately 19.9% below that of the as-sprayed coating, it was markedly higher than those obtained under the other UNSM conditions. Because only one tribological test was conducted for each condition, these cross-sectional areas are treated as individual comparative measurements rather than statistically averaged wear values. In addition, the wear-track width and maximum depth were not independently quantified. Therefore, the cross-sectional area is used here as an integral geometrical measure of the transverse wear profile. The detailed groove geometry cannot be reconstructed from this parameter alone, and the interpretation of wear

mechanisms was consequently based on the combined analysis of the profilometric data and the SEM/EDS morphology of the worn surfaces.

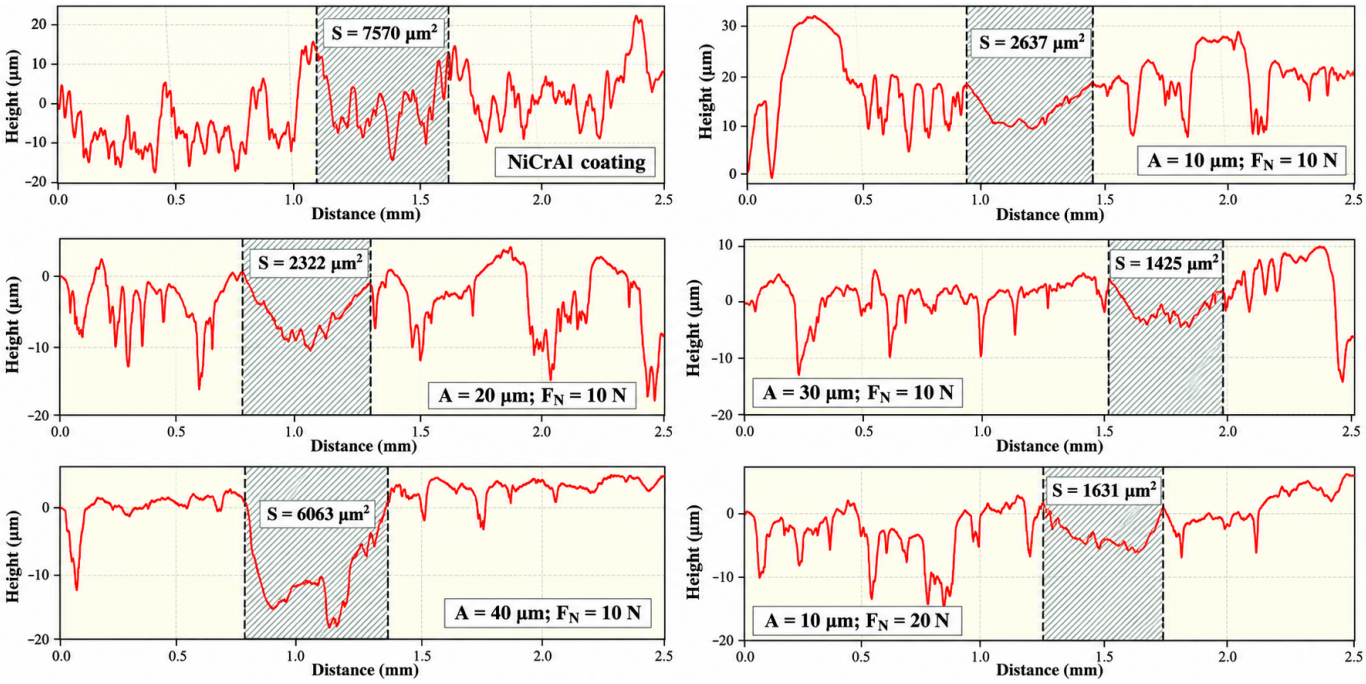


Figure 10. Wear-track profiles and corresponding cross-sectional areas of the detonation-sprayed NiCrAl coatings before and after UNSM treatment.

The comparative SEM images of the wear tracks are presented in Figure 11. The as-sprayed coating exhibits a strongly heterogeneous worn surface containing broad plastically deformed regions, fragmented areas, local cracking, and evidence of material removal. The characteristic lamellar heterogeneity of the initial coating remains visible within the worn region, indicating that sliding promotes progressive fracture and removal of locally weak surface asperities and splat-related regions. This morphology is consistent with the largest measured wear-track cross-sectional area. After A10F10 and A20F10 treatment, the worn surfaces remain heterogeneous but exhibit less extensive material removal than the as-sprayed coating. Local plastically deformed regions, microcracks, and fragmented areas are still observed; however, the wear scars appear comparatively more compact. These observations are consistent with the decrease in wear-track area from 7570 µm^2 in the as-sprayed state to 2637 and 2322 µm^2 after A10F10 and A20F10, respectively. Thus, moderate UNSM treatment improves resistance to material removal while not completely suppressing damage associated with the heterogeneous lamellar structure. The A30F10 condition exhibits the most favorable wear-track morphology among the investigated states. The worn region is comparatively compact, while extensive material pull-out and large opened discontinuities are less pronounced. Local plastic deformation and fine cracking remain present, but the coating maintains a more continuous load-bearing surface within the tribological contact. This morphology agrees with the minimum wear-track cross-sectional area of 1425 µm^2. The improved wear resistance of A30F10 can therefore be associated with the combined effects of reduced initial surface roughness, mechanical consolidation of the near-surface region, retention of hardness comparable to the as-sprayed coating within the experimental scatter, and preservation of sufficient inter-splat integrity. A different response is observed for A40F10. Although this condition produced the lowest initial roughness, Ra = 0.25 µm, the wear track contains more pronounced crack-like discontinuities, fragmented regions, and evidence of local material detachment. These observations

correlate with the marked decrease in hardness to 397 ± 98 HV and with the more pronounced inter-splat and subsurface discontinuities observed in the coating cross-section. Therefore, the minimum surface roughness obtained under A40F10 does not correspond to the maximum wear resistance. At this treatment intensity, severe surface smoothing is accompanied by deterioration of the local mechanical integrity of the heterogeneous lamellar coating, which facilitates crack propagation and fragment removal during sliding. For A10F20, the worn surface also contains pronounced plastically deformed and crack-like regions, indicating that increasing the normal load from 10 to 20 N intensifies mechanical interaction with structurally weak regions of the coating. Nevertheless, the measured wear-track area remains relatively low at 1631 μm^2. Thus, the higher normal load produces competing effects: it promotes substantial surface modification and resistance to material removal, while simultaneously increasing the tendency for local defect activation. This interpretation is consistent with the marked decrease in both hardness and elastic modulus observed for A10F20.

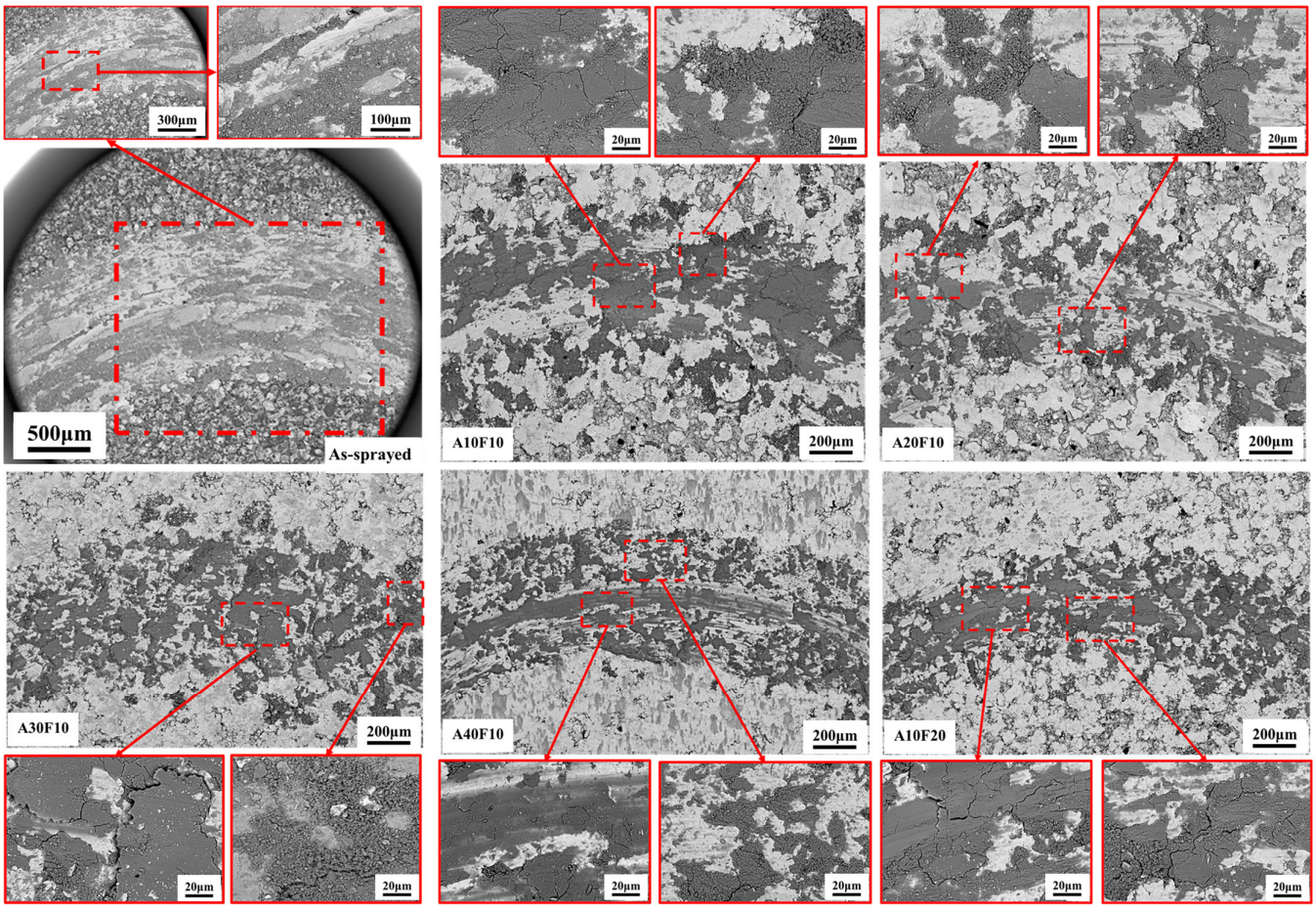


Figure 11. Comparative SEM/BSE images of the wear tracks of the detonation-sprayed NiCrAl coating: as-sprayed; A10F10; A20F10; A30F10; A40F10; and A10F20. Enlarged images show representative regions of plastic deformation, cracking, fragmentation, and local material removal.

The EDS elemental distribution maps of the wear tracks are presented in Figures 12 and 13. For the as-sprayed coating and all UNSM-treated conditions, the principal coating elements remain detectable throughout the investigated wear scars. The elemental maps show heterogeneous local distributions associated with the multiphase and lamellar character of the NiCrAl coating and with mechanical redistribution during sliding. Importantly, the maps do not indicate extensive exposure of the Fe-containing substrate over the investigated wear-track regions. This confirms that the differences in wear-track

morphology primarily reflect different degrees of deformation, fragmentation, and local material removal within the coating rather than complete through-thickness removal of the NiCrAl layer. Comparison of the SEM and EDS results with the profilometric data demonstrates that the wear behavior is governed by competition between beneficial surface modification and damage accumulation. In the as-sprayed state, the rough and structurally heterogeneous surface promotes fracture of asperities, fragmentation, and material removal, resulting in the largest wear-track area despite the lowest coefficient of friction. Moderate UNSM reduces the susceptibility of the surface to extensive material removal by smoothing and mechanically consolidating the near-surface region. The most favorable balance is achieved for A30F10, where substantial surface smoothing is obtained without the pronounced reduction in hardness observed under the more severe treatment conditions. Further increasing the ultrasonic amplitude to A40F10 or increasing the normal load to 20 N promotes stronger activation of inherited inter-splat and subsurface discontinuities. Under A40F10, this damage becomes sufficiently pronounced to substantially reduce the beneficial effect of surface smoothing on wear resistance. Accordingly, the tribological response of the detonation-sprayed NiCrAl coating is determined not by surface roughness, hardness, or friction coefficient individually, but by their combined relationship with the integrity of the heterogeneous lamellar structure. Among the investigated UNSM conditions, A30F10 provides the most favorable balance between surface smoothing, preservation of the local load-bearing response, inter-splat integrity, and resistance to material removal.

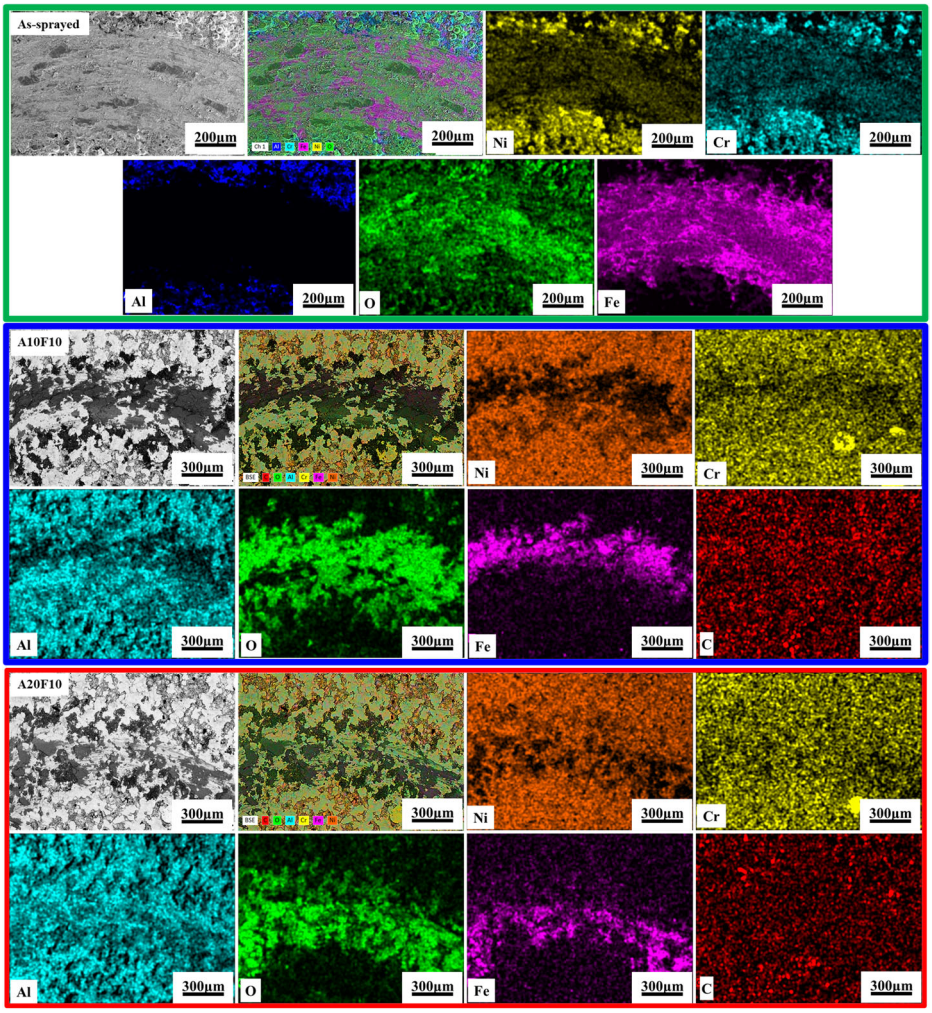


Figure 12. BSE images and EDS elemental distribution maps of the wear tracks of the detonation-sprayed NiCrAl coating: as-sprayed; A10F10; and A20F10.

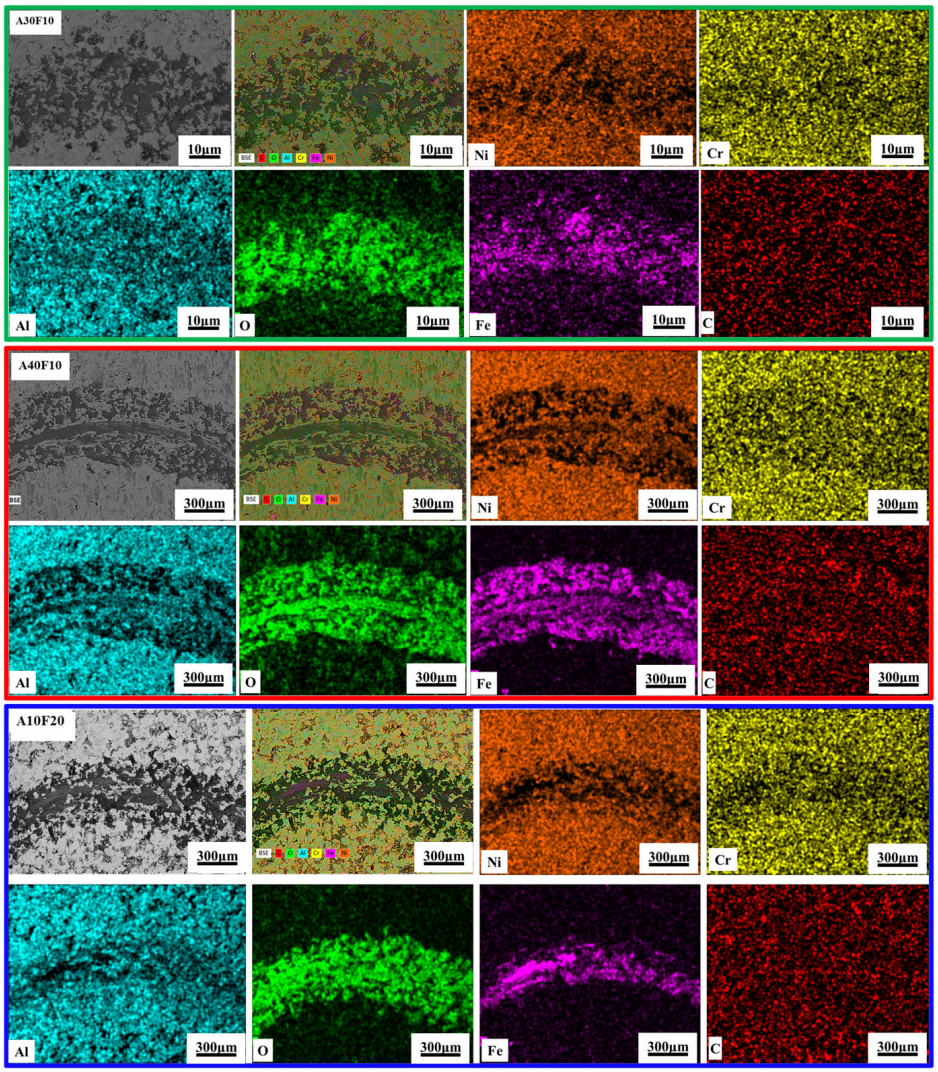


Figure 13. BSE images and EDS elemental distribution maps of the wear tracks of the detonation-sprayed NiCrAl coating after UNSM treatment: A30F10; A40F10; and A10F20.

4. Conclusions

The effect of ultrasonic nanocrystalline surface modification (UNSM) on the structural-phase state, morphology, and mechanical and tribological properties of a detonation-sprayed NiCrAl coating was investigated. It was shown that UNSM treatment significantly alters the state of the near-surface layer, with the nature of the changes determined by the combination of amplitude and normal load.

The treatment leads to a pronounced reduction in surface roughness. For the as-sprayed NiCrAl coating, the average Ra value was 3.78 μm. After A10F10 and A20F10, it decreased to 2.40 μm and after A30F10 to 1.94 μm, while the minimum roughness of 0.25 μm was obtained after A40F10. Increasing the normal load to 20 N at an amplitude of 10 μm also resulted in significant surface smoothing to Ra = 0.81 μm. The reduction in roughness is consistent with repeated impact-induced plastic deformation and flattening of surface asperities; however, the detailed peak-to-valley evolution cannot be resolved from the Ra data alone.

X-ray diffraction showed that the principal AlNi, Al_4Ni_3, and $AlCr_2$ phases were retained after UNSM treatment, while weak Al_3Ni_5 reflections were additionally observed under the A40F10 condition. After UNSM, changes in the shape and width of the diffraction peaks were observed, indicating predominantly deformation-induced restructuring of the

crystal structure. These changes may be associated with the accumulation of microstrains, an increase in defect density, and refinement of the coherent scattering domains without a fundamental change in the main phase composition of the coating.

SEM and EDS analyses showed that a clear interface between the NiCrAl coating and the Fe-containing substrate was retained after all investigated treatment conditions. Ni, Al, and Cr were predominantly localized in the coating, whereas Fe was concentrated in the substrate. With increasing UNSM intensity, the prominence of inter-splat and subsurface defects increased. Extended discontinuities and local crack-like regions were particularly pronounced under A40F10 and A10F20, indicating competition between surface compaction and the accumulation of structural damage.

The microhardness and elastic modulus results showed a non-monotonic change in the mechanical response of the coating. The as-sprayed coating exhibited a hardness of 623 ± 77 HV. The mean values measured after A20F10 and A30F10 were 660 ± 95 and 656 ± 189 HV, respectively; however, these differences were small relative to the corresponding standard deviations and therefore were not interpreted as statistically significant hardening. In contrast, the A40F10 and A10F20 conditions showed markedly lower mean hardness values of 397 ± 98 and 381 ± 139 HV, respectively. For A20F10, A30F10, and A40F10, the elastic modulus remained within the experimental scatter of the as-sprayed value of 121 ± 12 GPa. In contrast, A10F20 exhibited a markedly lower mean elastic modulus of 92 ± 14 GPa, corresponding to an approximately 24% reduction and indicating a substantial decrease in the local elastic stiffness and structural integrity of the coating. These results indicate that moderate UNSM conditions largely preserve the local indentation response of the coating, whereas more severe treatment conditions are associated with deterioration of the local mechanical response, expressed by reduced hardness and, for A10F20, a marked decrease in elastic modulus.

Tribological tests showed that after UNSM, the coefficient of friction increases compared with the as-sprayed NiCrAl coating; however, the wear resistance increases significantly. The cross-sectional area of the wear track of the as-sprayed coating was 7570 μm^2. After A10F10 and A20F10, it decreased to 2637 and 2322 μm^2, respectively. The smallest wear-track area was obtained at A30F10—1425 μm^2, corresponding to a reduction in wear of approximately 81% compared with the as-sprayed state. For A10F20, the value was 1631 μm^2, whereas at A40F10 the wear increased to 6063 μm^2, although it remained below the initial level.

SEM/EDS analysis of the wear tracks confirmed that UNSM changes the wear mechanism by suppressing extensive asperity fracture and material removal under moderate treatment conditions, while excessive amplitude or normal load promotes crack opening, inter-splat separation, and local fragmentation. The A30F10 condition exhibited the most favorable wear-track morphology, confirming that its superior wear resistance results from the combined effects of surface smoothing, retention of the local load-bearing response, and sufficient inter-splat integrity.

The obtained results indicate the existence of an optimal range of UNSM intensity for the detonation-sprayed NiCrAl coating. At lower treatment intensity, the mechanical modification of the coating is limited, whereas an excessive increase in amplitude or normal load promotes the opening of inter-splat defects and reduces the mechanical stability of the coating. The most favorable combination of structural state, retained hardness, and wear resistance was obtained for the A30F10 condition, which exhibited a hardness comparable to that of the as-sprayed coating within the experimental scatter together with the minimum wear-track area.

Author Contributions: Conceptualization, M.M. and Z.S.; methodology, M.M.; software, M.M.; validation, M.M., Z.S. and N.N.Y.; formal analysis, M.M.; investigation, N.N.Y.; resources, Z.S.; data curation, N.N.Y.; writing—original draft preparation, M.M.; writing—review and editing, M.M.; visualization, M.M.; supervision, Z.S.; project administration, M.M.; funding acquisition, M.M. All authors have read and agreed to the published version of the manuscript.

Funding: This research has been funded by the Committee of Science of the Ministry of Science and Higher Education of the Republic of Kazakhstan (Grant No. AP22688426).

Institutional Review Board Statement: Not applicable.

Informed Consent Statement: Not applicable.

Data Availability Statement: The original contributions presented in the study are included in this article; further inquiries can be directed to the corresponding author.

Conflicts of Interest: The authors declare no conflict of interest.

References

1. Kamal, S.; Jayaganthan, R.; Prakash, S.; Kumar, S. Hot corrosion behavior of detonation gun sprayed Cr_3C_2–NiCr coatings on Ni- and Fe-based superalloys in Na_2SO_4–60% V_2O_5 environment at 900 °C. *J. Alloys Compd.* **2008**, *463*, 358–372. [CrossRef]
2. Kamal, S.; Jayaganthan, R.; Prakash, S. Evaluation of cyclic hot corrosion behaviour of detonation gun sprayed Cr_3C_2–25%NiCr coatings on nickel- and iron-based superalloys. *Surf. Coat. Technol.* **2009**, *203*, 1004–1013. [CrossRef]
3. Kamal, S.; Jayaganthan, R.; Prakash, S. High temperature oxidation studies of detonation sprayed Cr_3C_2–NiCr coating on Fe- and Ni-based superalloys in air under cyclic condition at 900 °C. *J. Alloys Compd.* **2009**, *472*, 378–389. [CrossRef]
4. Kaur, M.; Singh, H.; Prakash, S. Surface engineering analysis of detonation-gun sprayed Cr_3C_2–NiCr coating under high-temperature oxidation and oxidation–erosion environments. *Surf. Coat. Technol.* **2011**, *206*, 530–541. [CrossRef]
5. Murthy, J.K.N.; Venkataraman, B. Abrasive wear behaviour of WC–CoCr and Cr_3C_2–20(NiCr) deposited by HVOF and detonation spray processes. *Surf. Coat. Technol.* **2006**, *200*, 2642–2652. [CrossRef]
6. Park, S.Y.; Kim, M.C.; Park, C.G. Mechanical properties and microstructure evolution of the nano WC–Co coatings fabricated by detonation gun spraying with post heat treatment. *Mater. Sci. Eng. A* **2007**, *449–451*, 894–897. [CrossRef]
7. Babu, P.S.; Basu, B.; Sundararajan, G. Processing–structure–property correlation and decarburization phenomenon in detonation sprayed WC–12Co coatings. *Acta Mater.* **2008**, *56*, 5012–5026. [CrossRef]
8. Du, H.; Hua, W.; Liu, J.; Gong, J.; Sun, C.; Wen, L. Influence of process variables on the qualities of detonation gun sprayed WC–Co coatings. *Mater. Sci. Eng. A* **2005**, *408*, 202–210. [CrossRef]
9. Sundararajan, G.; Sen, D.; Sivakumar, G. The tribological behaviour of detonation sprayed coatings: The importance of coating process parameters. *Wear* **2005**, *258*, 377–391. [CrossRef]
10. Rakhadilov, B.; Maulet, M.; Abilev, M.; Sagdoldina, Z.; Kozhanova, R. Structure and tribological properties of Ni–Cr–Al-based gradient coating prepared by detonation spraying. *Coatings* **2021**, *11*, 218. [CrossRef]
11. Rakhadilov, B.K.; Buitkenov, D.B.; Kabdykenova, E.; Sagdoldina, Z.B.; Zhurerova, L.G. Effect of the detonation-spraying mode on the tribological properties of NiCr–Al_2O_3 coatings. *Eurasian J. Phys. Funct. Mater.* **2021**, *5*, 39–44. [CrossRef]
12. Zhu, Z.; Wei, L.; Chen, J.; Cheng, J.; Chen, W.; Zhu, S.; Yang, J. Tribological behavior of NiCrAlY/Al_2O_3/h-BN metal-ceramic composite coatings at wide temperature range by detonation spraying. *Wear* **2024**, *550–551*, 205421. [CrossRef]
13. Sagdoldina, Z.; Rakhadilov, B.; Maulet, M.; Sulyubayeva, L.; Drenda, C.; Bolatov, S. Comprehensive Study of the Mechanical and Tribological Properties of NiCr-Al Detonation Coatings. *Appl. Sci.* **2025**, *15*, 7513. [CrossRef]
14. Kishore, A.; John, M.; Ralls, A.M.; Jose, S.A.; Kuruveri, U.B.; Menezes, P.L. Ultrasonic nanocrystal surface modification: Processes, characterization, properties, and applications. *Nanomaterials* **2022**, *12*, 1415. [CrossRef]
15. Qin, H.; Ren, Z.; Zhao, J.; Ye, C.; Doll, G.L.; Dong, Y. Effects of ultrasonic nanocrystal surface modification on the wear and micropitting behavior of bearing steel in boundary lubricated steel–steel contacts. *Wear* **2017**, *392–393*, 29–38. [CrossRef]
16. Kim, M.S.; Jo, Y.K.; Park, S.H.; Shim, D.S. Application of ultrasonic nanocrystal surface modification for improving surface profile of DEDed AISI 316L. *J. Mech. Sci. Technol.* **2019**, *33*, 5659–5667. [CrossRef]
17. Amanov, A.; Karimbaev, R.M.; Berkebile, S.P. Effect of ultrasonic nanocrystal surface modification on wear mechanisms of thermally-sprayed WC–Co coating. *Wear* **2021**, *477*, 203873. [CrossRef]
18. Jo, Y.K.; Gil, Y.W.; Shim, D.S.; Pyun, Y.S.; Park, S.H. Control of local hardness gradient of metal surface by inclined surface treatment using ultrasonic nanocrystal surface modification. *Int. J. Precis. Eng. Manuf.-Green Technol.* **2021**, *8*, 533–546. [CrossRef]

19. Ye, C.; Telang, A.; Gill, A.S.; Suslov, S.; Idell, Y.; Zweiacker, K.; Wiezorek, J.M.K.; Zhou, Z.; Qian, D.; Mannava, S.R.; et al. Gradient nanostructure and residual stresses induced by ultrasonic nano-crystal surface modification in 304 austenitic stainless steel for high strength and high ductility. *Mater. Sci. Eng. A* **2014**, *613*, 274–288. [CrossRef]
20. Cherif, A.; Pyoun, Y.; Scholtes, B. Effects of ultrasonic nanocrystal surface modification on residual stress state and fatigue strength of AISI 304. *J. Mater. Eng. Perform.* **2010**, *19*, 282–286. [CrossRef]
21. Cao, X.J.; Pyoun, Y.S.; Murakami, R. Fatigue properties of a S45C steel subjected to ultrasonic nanocrystal surface modification. *Appl. Surf. Sci.* **2010**, *256*, 6297–6303. [CrossRef]
22. Yasuoka, M.; Wang, P.; Zhang, K.; Qiu, Z.; Kusaka, K.; Pyoun, Y.S.; Murakami, R.I. Improvement of the fatigue strength of SUS304 austenite stainless steel using ultrasonic nanocrystal surface modification. *Surf. Coat. Technol.* **2013**, *218*, 93–98. [CrossRef]
23. Gill, A.; Telang, A.; Mannava, S.R.; Qian, D.; Pyoun, Y.S.; Soyama, H.; Vasudevan, V.K. Comparison of mechanisms of advanced mechanical surface treatments in nickel-based superalloy. *Mater. Sci. Eng. A* **2013**, *576*, 346–355. [CrossRef]
24. Hong, S.J.; Hwang, G.H.; Han, W.K.; Kang, S.G. Cyclic oxidation behavior of Pt-modified aluminide coating treated with ultrasonic nanocrystal surface modification on Ni-based superalloy. *Surf. Coat. Technol.* **2011**, *205*, 2714–2723. [CrossRef]
25. Amanov, A.; Berkebile, S.P. Improvement in tribological behavior of thermal spray Cr_2O_3 and Cr_3C_2–NiCr coatings by ultrasonic nanocrystal surface modification. *Mater. Lett.* **2022**, *314*, 131919. [CrossRef]
26. Amanov, A.; Berkebile, S.P. Enhancement of sliding wear and scratch resistance of two thermally sprayed Cr-based coatings by ultrasonic nanocrystal surface modification. *Wear* **2023**, *512–513*, 204555. [CrossRef]
27. Amanov, A.; Berkebile, S.P. Effect of ultrasonic nanocrystal surface modification on fuel-lubricated wear mechanisms of thermal spray Al_2O_3–TiO_2 coating. *Wear* **2025**, *566–567*, 205882. [CrossRef]
28. Amanov, A. Wear resistance and adhesive failure of thermal spray ceramic coatings deposited onto graphite in response to ultrasonic nanocrystal surface modification technique. *Appl. Surf. Sci.* **2019**, *477*, 184–197. [CrossRef]
29. Amanov, A. Surface engineering-controlled tribological behavior and adhesion strength of Ni–Cr coating sprayed onto carburized AISI 4340 steel substrate. *Surf. Coat. Technol.* **2019**, *370*, 144–156. [CrossRef]
30. Li, H.; Shen, W.; He, W.; Jiao, L.; Zhang, C.; Song, Z.; Wang, J.; Nie, Z.; Shcheretskyi, O. Preparation of AlCoCrFeNi HEA wear-resistant coatings by laser cladding on the surface of (ZrB_2 + Al_3Zr)/AA6016. *Mater. Today Commun.* **2025**, *48*, 113575.
31. Zhang, C.; Li, H.; Chen, S.; Jiao, L.; Shen, W.; Song, Z.; Wang, J.; Nie, Z.; Shcheretskyi, O. Preparation of graphene nanoplatelets reinforced aluminum matrix composites by friction stir processing and study of thermal conductivity and toughness properties. *Mater. Today Commun.* **2025**, *48*, 113606. [CrossRef]
32. Li, H.; Zhang, C.; Han, X.; Jiao, L.; Shen, W.; Song, Z.; Wang, J.; Nie, Z.; Shcheretskyi, O. Study on microstructural evolution and strengthening-toughening mechanisms of aluminum matrix composites fabricated by hot rolling and friction stir processing. *J. Mater. Sci.* **2025**, *60*, 15064–15086. [CrossRef]
33. *ISO 4955:2016*; Heat-Resistant Steels. International Organization for Standardization: Geneva, Switzerland, 2016.
34. *ASTM E2109-01(2021)*; Standard Test Methods for Determining Area Percentage Porosity in Thermal Sprayed Coatings. ASTM International: West Conshohocken, PA, USA, 2021.
35. Ulianitsky, V.Y.; Dudina, D.V.; Shtertser, A.; Smurov, I. Computer-controlled detonation spraying: Flexible control of the coating chemistry and microstructure. *Metals* **2019**, *9*, 1244. [CrossRef]
36. Aringozhina, Z.; Magazov, N.M.; Rakhadilov, B.K.; Uazyrkhanova, G.K.; Amanov, A. Effect of ultrasonic nanocrystalline surface modification on hardness and elastic modulus of Ti-6Al-4V alloy. *AIMS Mater. Sci.* **2025**, *12*, 101–117. [CrossRef]
37. Aringozhina, Z.; Rakhadilov, B.; Askhatov, A.; Adilkanova, M.; Magazov, N. Investigation of the Effect of Preliminary Mechanical Treatment on the Mechanical Properties of 12Kh18N10T Stainless Steel After Ion-Plasma Nitriding. *Materials* **2026**, *19*, 1960. [CrossRef]
38. *ASTM G99-23*; Standard Test Method for Wear and Friction Testing with a Pin-on-Disk or Ball-on-Disk Apparatus. ASTM International: West Conshohocken, PA, USA, 2023.
39. *ISO 13565-1:1996*; Geometrical Product Specifications (GPS)—Surface Texture: Profile Method; Surfaces Having Stratified Functional Properties—Part 1: Filtering and General Measurement Conditions. International Organization for Standardization: Geneva, Switzerland, 1996.
40. Polonyankin, D.A.; Fedorov, A.A.; Gomonyuk, T.M. Phase composition of stainless steel subjected to ultrasonic nanocrystal surface modification with different processing density. *J. Adv. Mater. Technol.* **2024**, *9*, 257–266. [CrossRef]

Disclaimer/Publisher's Note: The statements, opinions and data contained in all publications are solely those of the individual author(s) and contributor(s) and not of MDPI and/or the editor(s). MDPI and/or the editor(s) disclaim responsibility for any injury to people or property resulting from any ideas, methods, instructions or products referred to in the content.